

AEDC-TR-09-T-13



Plume Visualization of Orion Launch Abort Vehicle Jettison Motors Using Background-Oriented Schlieren

**Carrie K. Reinholtz, Fred L. Heltsley, and Kenneth E. Scott
Aerospace Testing Alliance**

January 2010

Final Report for Period 1 – 16 June 2009

Statement A: Approved for public release; distribution is unlimited.

**ARNOLD ENGINEERING DEVELOPMENT CENTER
ARNOLD AIR FORCE BASE, TENNESSEE
AIR FORCE MATERIEL COMMAND
UNITED STATES AIR FORCE**

NOTICES

When U. S. Government drawings, specifications, or other data are used for any purpose other than a definitely related Government procurement operation, the Government thereby incurs no responsibility nor any obligation whatsoever, and the fact that the Government may have formulated, furnished, or in any way supplied the said drawings, specifications, or other data, is not to be regarded by implication or otherwise, as in any manner licensing the holder or any other person or corporation, or conveying any rights or permission to manufacture, use, or sell any patented invention that may in any way be related thereto.

Qualified users may obtain copies of this report from the Defense Technical Information Center.

References to named commercial products in this report are not to be considered in any sense as an endorsement of the product by the United States Air Force or the Government.

DESTRUCTION NOTICE

For unclassified, limited documents, destroy by any method that will prevent disclosure or reconstruction of the document.

APPROVAL STATEMENT

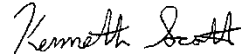
Prepared by:



CARRIE K. REINHOLTZ
Aerospace Testing Alliance



FRED L. HELTSLEY
Aerospace Testing Alliance



KENNETH E. SCOTT
Aerospace Testing Alliance

Reviewed by:



WINFORD C. PHIPPS
Air Force Project Manager
716th Test Squadron

Approved by:



JOHN J. WALTERS
Deputy Director
716th Test Squadron

REPORT DOCUMENTATION PAGE				Form Approved OMB No. 0704-0188	
<p>The public reporting burden for this collection of information is estimated to average 1 hour per response, including the time for reviewing instructions, searching existing data sources, gathering and maintaining the data needed, and completing and reviewing the collection of information. Send comments regarding this burden estimate or any other aspect of this collection of information, including suggestions for reducing the burden, to Department of Defense, Washington Headquarters Services, Directorate for Information Operations and Reports (0704-0188), 1215 Jefferson Davis Highway, Suite 1204, Arlington, VA 22202-4302. Respondents should be aware that notwithstanding any other provision of law, no person shall be subject to any penalty for failing to comply with a collection of information if it does not display a currently valid OMB control number.</p> <p>PLEASE DO NOT RETURN YOUR FORM TO THE ABOVE ADDRESS</p>					
1. REPORT DATE (DD-MM-YYYY) xx-01-2010		2. REPORT TYPE Final		3. DATES COVERED (From – To) 1-16 June 2009	
4. TITLE AND SUBTITLE Plume Visualization of NASA CEV Jettison Motors Using Background-Oriented Schlieren			5a. CONTRACT NUMBER		
			5b. GRANT NUMBER		
			5c. PROGRAM ELEMENT NUMBER		
6. AUTHOR(S) Reinholtz, C. K., Heltsley, F. L, and Scott, K. E. Aerospace Testing Alliance			5d. PROJECT NUMBER 12696		
			5e. TASK NUMBER		
			5f. WORK UNIT NUMBER		
7. PERFORMING ORGANIZATION NAME(S) AND ADDRESS(ES) Arnold Engineering Development Center/716 th Test Squadron				8. PERFORMING ORGANIZATION REPORT NO. AEDC-TR-09-T-13	
9. SPONSORING/MONITORING AGENCY NAME(S) AND ADDRESS(ES) NASA Johnson Space Center Mail Code: EG3 2101 NASA Parkway Houston, TX 77058				10. SPONSOR/MONITOR'S ACRONYM(S) NASA JSC	
				11. SPONSOR/MONITOR'S REPORT NUMBER(S)	
12. DISTRIBUTION/AVAILABILITY STATEMENT Statement A: Approved for public release; distribution is unlimited.					
13. SUPPLEMENTARY NOTES Available in the Defense Technical Information Center (DTIC).					
14. ABSTRACT A background-oriented schlieren (BOS) system has recently been implemented in the Aerodynamic Wind Tunnel 16T at Arnold Engineering Development Center (AEDC) to qualitatively visualize the jettison motor plumes on the NASA Crew Exploration Vehicle (CEV). As applied to aerodynamics, BOS is an optical technique that exploits gradients in the refractive index of fluid volumes like schlieren, shadowgraph, and interferometry techniques to visualize flow structures and density gradients. BOS requires only small optical accesses to view a painted dot pattern through a refracting media to visualize density gradients in the fluid. This is of particular interest in wind tunnels or other testing facilities where optical access is limited and/or other common visualization techniques are not readily available. Images were acquired for multiple Mach number flows, plenum pressures and model attitudes to visualize the jet plume and model shock interactions for two Jettison Motor geometries.					
15. Subject Terms jettison motor, high-pressure air, plume interaction, separation, crew module, launch abort tower, ARES I Launch Vehicle, abort, re-entry phase, wind tunnel test, AEDC Propulsion Wind Tunnel 16T, transonic, reverse freestream flow, background-oriented schlieren, plume visualization.					
16. SECURITY CLASSIFICATION OF:			17. LIMITATION OF ABSTRACT	18. NUMBER OF PAGES	19A. NAME OF RESPONSIBLE PERSON
A. REPORT	B. ABSTRACT	C. THIS PAGE			19B. TELEPHONE NUMBER (Include area code)
Unclassified	Unclassified	Unclassified	Same as Report	53	Mr. Winford C. Phipps (931) 454-3011

PREFACE

The work reported herein was conducted by the Arnold Engineering Development Center (AEDC), Air Force Materiel Command (AFMC), at the request of the NASA Johnson Space Center Mail Code: EG3 2101 NASA Parkway Houston, TX 77058. The Sponsor project manager was Mr. Tuan H. Truong of NASA JSC. The Customer representative was Mr. Matthew C. Rhode of the NASA Langley Research Center, Mail Stop 408A, Hampton, VA 23681. The test results were obtained by Aerospace Testing Alliance (ATA), the operations, maintenance, information management, and support contractor for AEDC, AFMC, Arnold Air Force Base, TN 37389. The ATA project manager was Mr. Charles L. Smith. The test was conducted in the Propulsion Wind Tunnel (PWT) 16T of the PWT Facility during the period from 1 – 16 June 2009 under AEDC Job Number 12696, PWT Test Number TF-1045.

CONTENTS

		<u>Page</u>
1.0	INTRODUCTION.....	5
2.0	APPARATUS	5
2.1	Test Facility	5
2.2	Test Article	6
2.3	Background-Oriented Schlieren Theory	6
2.4	Background-Oriented Schlieren Technique.....	6
2.5	Background-Oriented Schlieren Data System.....	7
3.0	PROCEDURES.....	7
3.1	Test Conditions	7
3.2	Data Acquisition	7
3.3	Data Reduction.....	8
4.0	RESULTS AND DISCUSSION.....	8
5.0	SUMMARY	9
	REFERENCES.....	10

FIGURES

Figure

1.	Launch Abort System Test Article Details.....	11
2.	Crew Exploration Vehicle Test Article Installed in Tunnel 16T HAAS Cart.	12
3.	BOS System Configuration	13
4.	BOS System Schematic Looking Downstream	14
5.	BOS Installation Photos	15
6.	Close-Up Image of BOS Dot Pattern Applied to East Wall	16
7.	Large JM (PTJM = avg) Nozzle BOS Visualization During Configuration 101 High-Pressure Air Checkout and Simulated Schlieren Images for a Multipass Processor Using a 32 x 32 Pixel Region at 50% Overlap Down to a 16 x 16 Pixel Region at 87% Overlap	17
8.	Large JM Nozzle (PTJM = avg) BOS Visualization During Configuration 101 High-Pressure Air Checkout and Simulated Schlieren Images for a Multipass Processor Using a 64 x 64 Pixel Region at 75% Overlap Down to a 32 x 32 Pixel Region at 87% Overlap	17

9. Small JM (PTJM = avg) Nozzle BOS Visualization During Configuration 101 High-Pressure Air Checkout and Simulated Schlieren Images for a Multipass Processor Using a 32 x 32 Pixel Region at 50% Overlap Down to a 16 x 16 Pixel Region at 87% Overlap	18
10. Small JM Nozzle (PTJM = avg) BOS Visualization During Configuration 101 High-Pressure Air Checkout and Simulated Schlieren Images for a Multipass Processor Using a 64 x 64 Pixel Region at 75% Overlap Down to a 32 x 32 Pixel Region at 87% Overlap	18
11. BOS Visualization of C101 Large JM Nozzle (PTJM = avg) at Mach 0.7 and 4 Model Attitudes. Processed with Mach 0.7 Jet-Off Background Image	19
12. BOS Visualization of C101 Small JM Nozzle (PTJM = avg) at Mach 0.7 and 4 Model Attitudes. Processed with Mach 0.7 Jet-Off Background Image	20
13. BOS Visualization of C103 Large JM Nozzle (PTJM = avg) at Mach 0.5 and 4 Model Attitudes. Processed with Mach 0.5 Jet-Off Background Image	21
14. BOS Visualization of C103 Small JM Nozzle (PTJM = avg) at Mach 0.5 and 4 Model Attitudes. Processed with Mach 0.5 Jet-Off Background Image	22
15. BOS Visualization of C103 Large JM Nozzle (PTJM = avg) at Mach 0.9 and 4 Model Attitudes. Processed with Mach 0.9 Jet-Off Background Image	23
16. BOS Visualization of C103 Small JM Nozzle (PTJM = avg) at Mach 0.9 and 4 Model Attitudes. Processed with Mach 0.9 Jet-Off Background Image	24
17. BOS Visualization of C103 Large JM Nozzle (PTJM = avg) at Mach 1.2 and 4 Model Attitudes. Processed with Mach 1.2 Jet-Off Background Image	25
18. BOS Visualization of C103 Small JM Nozzle (PTJM = avg) at Mach 1.2 and 4 Model Attitudes. Processed with Mach 1.2 Jet-Off Background Image	26
19. BOS Visualization of C105 Large JM Nozzle (PTJM = avg) at Mach 0.9 and 2 Model Attitudes. Processed with Mach 0.9 Jet-Off Background Image	27
20. BOS Visualization of C105 Small JM Nozzle (PTJM = avg) at Mach 0.9 and 2 Model Attitudes. Processed with Mach 0.9 Jet-Off Background Image	27
21. BOS Visualization of C105 Large JM Nozzle (PTJM = avg) at Mach 1.2 and 4 Model Attitudes. Processed with Mach 1.2 Jet-Off Background Image	28
22. BOS Visualization of C105 Small JM Nozzle (PTJM = avg) at Mach 1.2 and 2 Model Attitudes. Processed with Mach 1.2 Jet-Off Background Image	29
23. BOS Visualization of C106 Small JM Nozzle (PTJM = avg) at Mach 0.9 and 2 Model Attitudes. Image (a) was Processed Using the Atmosphere Jet-Off Background Image Due to Model Dynamics, While Image (b) Used the Mach 0.9 Jet-Off Background Image	29
24. BOS Visualization of C106 Large JM Nozzle (PTJM = avg) at Mach 0.9 and 4 Model Attitudes. Image (a) was Processed Using the Atmosphere Jet-Off Background Image Due to Model Dynamics. Images (b)-(d) were Processed Using the Mach 0.9 Jet-Off Background Image	30
25. BOS Visualization of C106 Large JM Nozzle (PTJM = avg) at Mach 1.2 and 4 Model Attitudes. Processed with Mach 1.2 Jet-Off Background Image	31

26. BOS Visualization of C106 Small JM Nozzle (PTJM = avg) at Mach 1.2 and 4 Model Attitudes. Processed with Mach 1.2 Jet-Off Background Image	32
27. BOS Visualization of C107 Large JM Nozzle (PTJM = avg) at Mach 0.9 and 4 Model Attitudes. Processed with Mach 0.9 Jet-Off Background Image	33
28. BOS Visualization of C107 Small JM Nozzle (PTJM = avg) at Mach 0.9 and 4 Model Attitudes. Processed with Mach 0.9 Jet-Off Background Image	34
29. BOS Visualization of C107 Large JM Nozzle (PTJM = avg) at Mach 1.2 and 4 Model Attitudes. Processed with Mach 1.2 Jet-Off Background Image	35
30. BOS Visualization of C107 Small JM Nozzle (PTJM = avg) at Mach 1.2 and 4 Model Attitudes. Processed with Mach 1.2 Jet-Off Background Image	36
31. BOS Visualization of C109 Large JM Nozzle at Mach 0.5 and Pitched to 170 deg for 3 Nozzle Pressures. Processed with Mach 0.5 Jet-Off Background Image	37
32. BOS Visualization of C109 Large JM Nozzle at Mach 0.9 and Pitched to 170 deg for 3 Nozzle Pressures. Processed with Mach 0.9 Jet-Off Background Image	38
33. BOS Visualization of C109 Large JM Nozzle at Mach 1.2 and Pitched to 170 deg for 3 nozzle Pressures. Processed with Mach 1.2 Jet-Off Background Image	39
34. BOS Visualization of C111 Large JM Nozzle at Mach 0.5 and Pitched to 170 deg for 3 Nozzle Pressures. Processed with Mach 0.5 Jet-Off Background Image	40
35. BOS Visualization of C111 Large JM Nozzle at Mach 0.9 and Pitched to 170 deg for 3 Nozzle Pressures. Processed with Mach 0.9 Jet-Off Background Image	41
36. BOS Visualization of C111 Large JM Nozzle at Mach 1.2 and Pitched to 170 deg for 3 Nozzle Pressures. Processed with Mach 1.2 Jet-Off Background Image	42

TABLES

Table

1. Nominal Test Conditions	43
2. Run Number Summary	43

APPENDICES

Appendix

A. Lamina BL3000 Series LED SPECIFICATION	45
B. Axon Retroreflective Paint	48
C. Photometrics CoolSNAP K4 Camera	51
NOMENCLATURE	53

1.0 INTRODUCTION

The background-oriented schlieren (BOS) data acquisition system in the Arnold Engineering Development Center's (AEDC) Propulsion Wind Tunnel (PWT) 16T was used to visualize the jettison motor (JM) plumes on a scaled NASA Orion Launch Abort System (LAS). The overall objective of this effort was to provide plume visualization of the NASA Crew Exploration Vehicle (CEV) Jettison Motors and their mutual interaction with the freestream flow. For this test a single optical port was used to accommodate a high-resolution CCD camera (4MP) and two white LED arrays. A pseudo-random pattern of 3/16-in. black dots applied over a 9- by 9-ft area of retroreflective paint on the opposite wall provided the image background texture required for BOS processing.

During testing, multiple air-on images were acquired at each selected test condition to record apparent distortion of a background dot pattern caused by flow-induced refractive index gradients within the test article flow field. Displacement vectors that indicate the direction and magnitude of flow-induced background pattern distortion were computed by cross-correlating each air-on image with an undistorted reference image acquired with the jets off. Standard Particle Image Velocimetry (PIV) software was used to calculate displacement vectors and create grayscale images that resemble schlieren photographs.

2.0 APPARATUS

2.1 TEST FACILITY

The AEDC Propulsion Wind Tunnel 16T is a closed-loop, continuous-flow, variable-density tunnel capable of being operated at Mach numbers from 0.06 to 1.60 and stagnation pressures from 120 to 4,000 psfa. The maximum attainable Mach number can vary slightly depending upon the tunnel pressure ratio requirements of a particular test installation. The maximum stagnation pressure attainable is a function of Mach number and available electric power. The tunnel stagnation temperature can be varied from approximately 60 to 160°F depending upon the available cooling water temperature. The tunnel is equipped with a scavenging system that removes combustion products when rocket motors or turbo-engines are being tested.

The high-angle automated sting (HAAS) cart was used during the test. It has a 16-ft-square by 40-ft-long test section enclosed by porous walls. The wall porosity is fixed at 6% and is provided by regularly spaced 0.75-in.-diam holes, which are inclined upstream at a 60-deg angle. The test section is completely enclosed in a plenum chamber from which air is evacuated at transonic and supersonic conditions, thus removing part of the tunnel airflow boundary layer through the porous walls of the test section. The HAAS test section has a sidewall angle variation capability from -2.0 deg (convergence) to 0.8 deg (divergence). To compensate for the HAAS strut blockage, each sidewall has a bulge section 6.0 in. deep. The model support system consisted of a pitch sector and sting attachment with a pitch capability from approximately -3 to 40 deg (position 2) with respect to the tunnel centerline and a roll capability of ± 180 deg about the sting centerline.

No conventional schlieren system is available in Tunnel 16T because of spatial restrictions and optical access limitations imposed by the porous walls. Additional information about Tunnel 16T, its capabilities, its operating characteristics, and its support systems is presented in Ref. 1.

2.2 TEST ARTICLE

The test article was a scaled model of the NASA Orion LAS including the Crew Module (CM), Boost Protective Cover (BPC), and Launch Abort Tower (LAT) as shown in Fig. 1. The model was mounted with the CM heat shield forward while simulating rocket plumes from the four JM ports located on the LAT with high-pressure air. Figure 2 shows the test article installed in the 16T HAAS cart. Several different model configurations were tested. Configuration 101 included the CM only, while configurations 103 through 111 incorporated different translations and pitch angularities of the CM with respect to the LAT.

2.3 BACKGROUND-ORIENTED SCHLIEREN THEORY

Just as in classical schlieren photography, background-oriented schlieren exploits the relationship between the density and refractive index of a gas. When a light ray passes through a medium with a refractive index gradient, the ray is bent in the direction of increasing density. The refractive index of a fluid can be related to the density by the empirical Gladstone-Dale equation

$$\frac{n-1}{\rho} = K_{G-D}, \quad (1)$$

where K_{G-D} , the Gladstone-Dale constant, is constant for a given gas (Refs. 2, 3), ρ is the density, and n is the index of refraction. The radius of curvature of a light ray passing through a gas can be expressed as inversely proportional to the gradient of the index of refraction, or

$$\frac{1}{R} = \nabla n, \quad (2)$$

where R is the radius of curvature and n is the index of refraction.

The deflected angle of the light ray, ε , is given by:

$$\varepsilon = \frac{L}{R} = LK_{G-D}\nabla\rho, \quad (3)$$

where L is the path length traveled by the light ray and $\nabla\rho$ is the density gradient. This relation shows that the deflection of the light ray is proportional to the density gradient of the medium through which it is travelling.

2.4 BACKGROUND-ORIENTED SCHLIEREN TECHNIQUE

The BOS technique differs from classical schlieren imagery in that images are acquired and then post-processed to visualize the density gradients in the flow field. Figure 3 is a conceptual drawing of the BOS installation showing the arrangement of the digital camera, LED light source, and East wall dot pattern relative to the test article. Two images of the dot pattern have to be acquired for BOS visualizations: one during a wind-off event (zero-density gradients) and a second during wind-on, or in the presence of density gradients and the associated background pattern distortion. Algorithms in standard Particle Image Velocimetry (PIV) software can be used to cross-correlate the two images and calculate the displacement vectors from the two images. The displacement vectors represent the local deflection of the light rays as they

pass through the gradients within the measurement volume. Plotting scalar values extracted from vector components allow schlieren-like images to be created. For the purpose of this test, BOS images were acquired for qualitative visualization.

2.5 BACKGROUND-ORIENTED SCHLIEREN DATA SYSTEM

A BOS system is comprised of four main components: a high-resolution digital camera, a light source, a painted dot pattern, and a data acquisition/analysis computer. Figure 4 shows a schematic of the BOS system installation. Installation photographs of the system components are presented in Fig. 5. The background pattern (Fig. 5a) consists of a 9- x 9-ft area of retroreflective paint applied to the tunnel east wall. Random black dots were then stamped on top of the retroreflective paint to provide a suitable background texture for the BOS images (Fig. 6). The dot size of approximately 3/16-in. diameter was chosen to appear as 3-5 pixel diameter dots when imaged to allow for subpixel accuracy during cross-correlation using PIV software (Ref. 4). One Photometrics® CoolSNAP™ K4 12-bit, interline transfer camera with 2,048 x 2,048 pixel spatial resolution was installed level with the test section centerline at a tunnel station 174 in. from the beginning of the test section (Fig. 2). At the expense of perspective distortion, the camera was angled approximately 12 deg both upstream and above the model in the tunnel. This arrangement provided a field of view approximately 4.5 x 4.5 ft around the CEV to visualize the JM jet plumes. The camera was outfitted with an 18-35 mm focal length zoom lens (f/5.6), and a 500- μ s exposure time was used to provide a sufficient contrast ratio. Two light sources, each configured with eight Lamina® BL-3000™ white LED arrays, were positioned above and below the camera to illuminate the retroreflective paint. Each LED array consisted of 39 individual cavities for a total of 624 LEDs. A PC with a single quad-core processor was used to control the cameras and data acquisition. The camera was connected to the computer via a PCI card and fiber optic cable. WinView32™ was used for image acquisition, while LaVision® DaVis™ software was used to process and export the final BOS videos and images.

3.0 PROCEDURES

3.1 TEST CONDITIONS

The test was conducted at a constant unit Reynolds number of 1.0 million/ft. The interaction of the model and the JM jet plumes was assessed for configurations 101-107 at Mach numbers of 0.5, 0.7, 0.9, and 1.2 for corresponding average jettison motor pressures (PTJM). For configurations 109 and 111, three different PTJM pressures were imaged corresponding to the minimum, maximum, and average nozzle pressure at one model attitude. The nominal test conditions established during the test are given in Table 1. Several test points were omitted due to model dynamics. A test run summary is presented in Table 2. Run numbers are tabulated in the appropriate Mach number column next to the associated test condition, model configuration, and model attitudes.

3.2 DATA ACQUISITION

BOS images were acquired for seven different model configurations under three circumstances; wind-off jet-off, wind-on jet-off at test condition, and wind-on jet-on at test condition. Selective postprocessing of these data points allows for jet-on and wind-on phenomena to be distinguished separately. This is especially useful in the transonic regime where flow may be locally accelerated and local supersonic regions become apparent around the test article. Sets of 5 background images were acquired for each model attitude at both jet-off conditions, and sets of 10 images were acquired for each model attitude at the jet-on condition, each at 1.5 Hz.

For each test condition the model was paused at each selected roll and pitch angle to allow the acquisition of multiple BOS images. Comparison of the large and small JM plumes was accomplished by rolling the model to -135 and -225 deg, respectively, and thus positioning each JM in turn on top of the model and in the BOS field of view. At each roll angle, images were acquired with the model pitched to angles of 180, 170, 160 and 150 deg. Images were stored based on the facility run and point numbers for association with the analogous test conditions.

3.3 DATA REDUCTION

Upon acquisition, each image set was stored as a single, 10-frame image file. For data reduction, the 10 image frames were separated into single images and converted to a standard 12-bit TIFF file. Each jet-on data set was paired with its appropriate jet-off wind-on background image and imported into DaVis™ for postprocessing. Alternately, wind-off jet-off images were used as background for processing the data in Figs 23a and 24a because model dynamics prevented the acquisition of wind-on jet-off data for those conditions. Additionally, only wind-off jet-off backgrounds were available for processing the wind-off jet-on images in Figs. 7 through 10. Once these files were imported, a batch processor was set up to 1) create wind-off/wind-on image pairs, 2) apply an image mask around the test article, 3) cross-correlate the image pairs using PIV algorithms, and 4) extract the scalar field for contour plots. A mask of each configuration and model attitude was created to reduce the number of stray and spurious vectors from around the edges of the test article. The mask also reduces the number of processed pixels, which slightly decreases the overall processing time.

For the data represented in Figs. 7 through 36, two main PIV processing schemes were employed. The first processing scheme was used during the high-pressure air checkout of the JMs (Figs. 7 through 10). This scheme used a multipass correlation algorithm with initial window size of 64 x 64 pixels at 75% overlap down to a final window size of 32 x 32 pixels at 87% overlap. The second processing scheme employed on the remaining data sets also used a multipass algorithm; however an initial interrogation volume of 32 x 32 pixels with 50% overlap was used and processed down to a 16 x 16 pixel region with 87% overlap. The second process (finer grid) resulted in data loss for the high-pressure air checkouts of the JMs because of the large density gradients in the plumes. Therefore, the first processing scheme was used and resulted in lower resolution images.

After each vector field was computed for each of the data sets, scalar fields were extracted. Density gradients were the strongest in the streamwise direction; therefore, the scalar fields representing vertical knife edge schlieren images are presented herein with the exception of the JM high-pressure air checkout. Both vertical and horizontally simulated schlieren images are presented in Figs. 7 through 10 for the JM to more clearly depict the shock diamond pattern within the plume.

4.0 RESULTS AND DISCUSSION

Figures 7 through 36 show a representative dataset from the BOS tunnel entry and include only a single image from each unique configuration and model attitude combination. The full dataset that was delivered to the customer includes all 10 images for each combination, presented both individually and as pseudo-video clips displayed at 1 Hz. The package also included additional images that were processed using wind-off jet-off data for background.

Prior to the wind-on runs, a series of images were acquired during the tunnel wind-off high-pressure air checkout to determine whether BOS would be feasible for visualization of the JM

plumes during the remainder of the test. Figures 7 through 10 show these results and confirm the applicability of the BOS system for plume visualization.

Figures 7 and 9 show the large and small JM plumes, respectively, for configuration 101, crew module (CM) only and show the shock diamonds as well as the upstream plume propagation. This image set was processed using a multipass processing scheme with initial interrogation region of 32 x 32 pixels and 50% overlap down to a 16 x 16 pixel region with 87% overlap. The images in Figs. 8 and 10 used a similar processor; however, they used an initial region of 64 x 64 pixels with 50% overlap down to a 32 x 32 pixel region with an overlap of 87%. Horizontal (a) and vertical (b) knife edge schlieren images were simulated during postprocessing to differentiate between vertical and horizontal density gradients. Note the resolution differences between Figs. 7 and 8 as well as Figs. 9 and 10 due to the finer grid processor used in Figs. 7 and 9. Although a finer grid may give more detail of the system, notice that the data fall out around the nozzle exit as indicated by the black pixels. Density gradients are extremely strong in this region, resulting in large displacements of the background dot pattern and violating the allowable displacement within an interrogation window. This violation results in a bad vector and missing data on the final BOS image. The problem is mitigated when processed using a larger window size.

Figures 11 through 30 show the JM nozzle plumes in flows of Mach 0.5, 0.7, 0.9, and 1.2 grouped in order of configuration number at the corresponding average jettison motor total pressures (PTJM). Small and large JM nozzle geometries were imaged for configurations 101 through 107. Due to model dynamics, several model attitudes had to be omitted. Jet-off images could not be captured for configuration 106 in Mach 0.9 flow and pitched to 180 deg due to model dynamics. Similarly, jet-on images at higher angles of attack could not be acquired in configurations 105 and 106 at Mach numbers of 0.9 and 1.2.

For configurations 109 and 111, only one model attitude was imaged for the large JM at 2 Mach numbers. Figures 31 through 36 show the minimum, maximum, and average pressure setting for the JMs in Mach 0.9 and 1.2 flows.

5.0 SUMMARY

The AEDC BOS data acquisition and analysis system has recently been improved and implemented for use in the 16-ft transonic wind tunnel. The improvements were demonstrated during the subject test performed in support of the Orion program. Background and wind-on image pairs of an optical dot pattern were acquired and cross-correlated using standard PIV data reduction techniques to provide plume visualization of the jettison motor jet plumes and their mutual interaction with the NASA CEV flow field.

The authors would like to acknowledge the work and support of the NASA CEV test team. A special thanks to Matt Rhode from NASA Langley; Chuck Niskey from Black Ram; Jim Ross, J.T. Heineck, and Louise Walker from NASA Ames; and Win Phipps, Charlie Smith, Reggie Riddle, and David Smith from AEDC. Without the assistance, patience, and expertise of these individuals, this test would not have been successful.

REFERENCES

1. *Test Facilities Handbook*, Vol. 4, "Propulsion Wind Tunnel Facility," Arnold Engineering Development Center, May 1992 (Thirteenth Edition).
2. Ladenburg, R. W., Lewis, B., Pease, R. N., and Taylor, H. S. *Physical Measurements in Gas Dynamics and Combustion*. Princeton University Press, New Jersey, 1954.
3. Shapiro, A. H. *The Dynamics and Thermodynamics of Compressible Fluid Flow*. John Wiley and Sons, New York, 1953.
4. Santiago, J. G., Wereley, S. T., Meinhart, C. D., Beebe, D. J. and Adrian, R. J., "A Particle Image Velocimetry System for Microfluidics," *Experiments in Fluids*. Vol. 25, 1998, pp. 316-319.

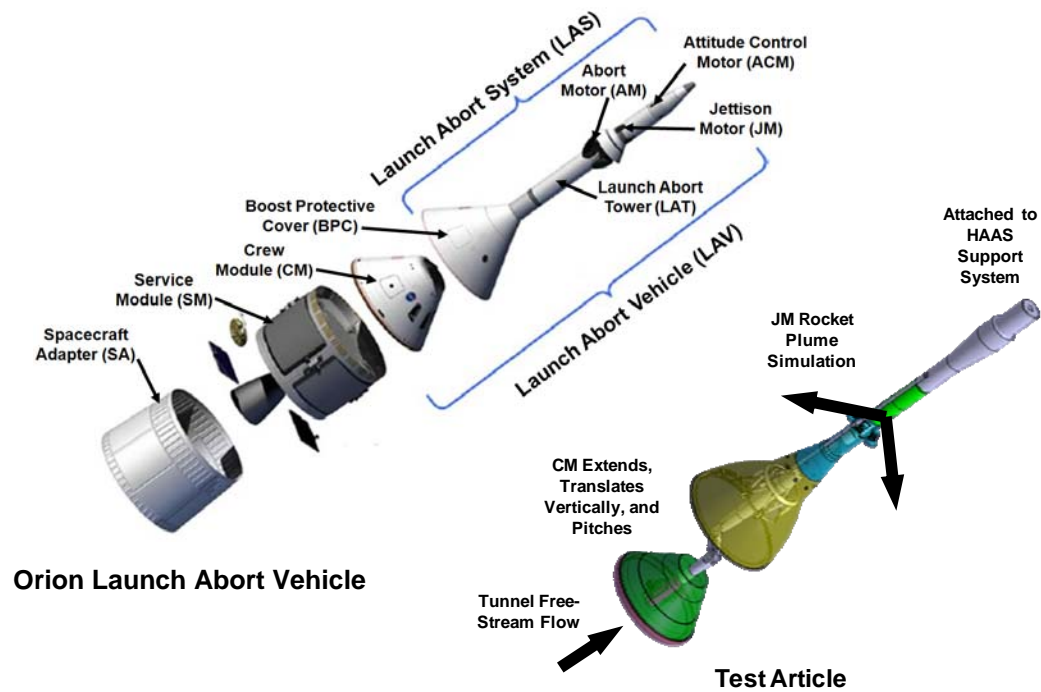


Figure 1. Launch Abort System Test Article Details.

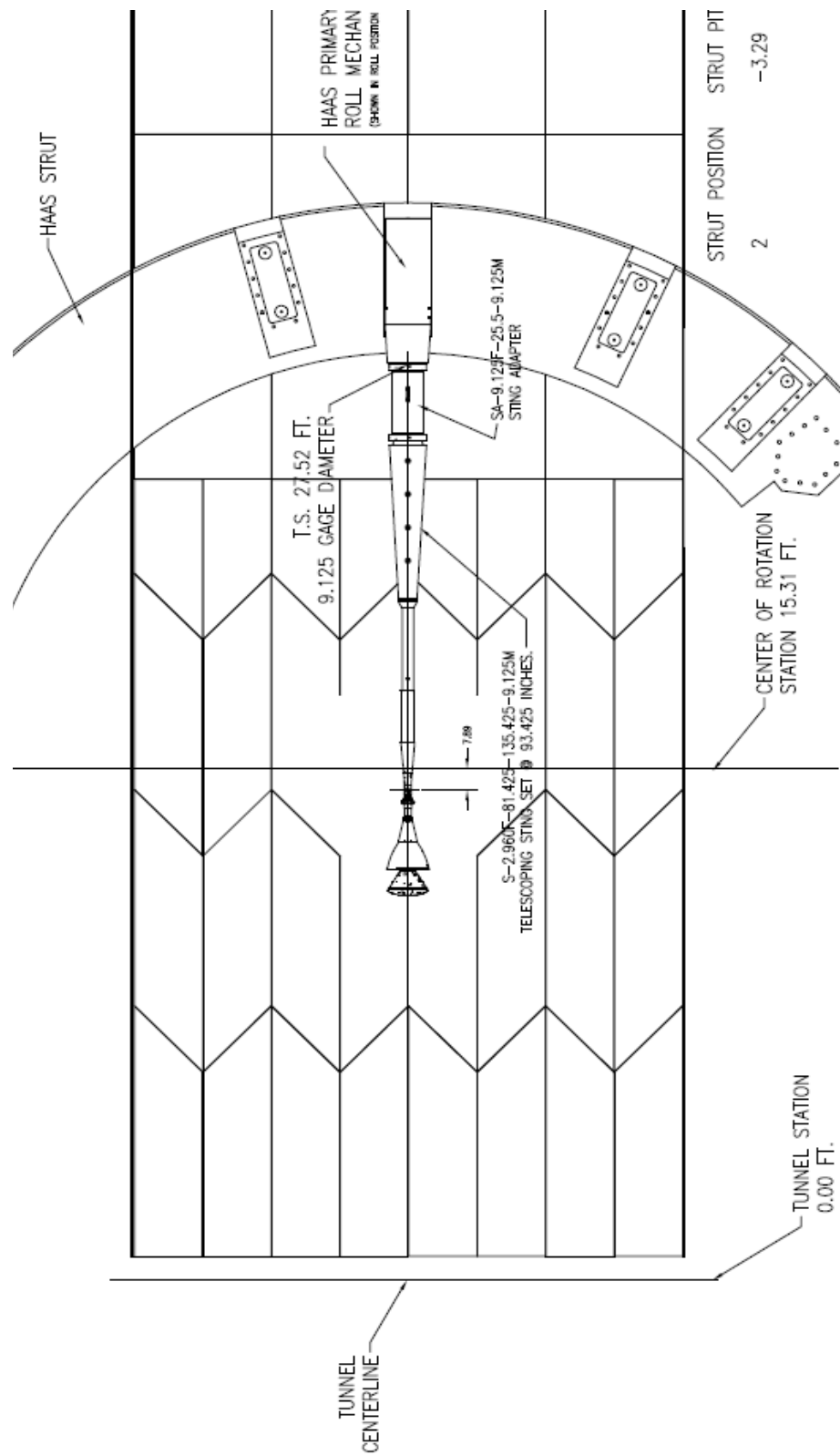


Figure 2. Crew Exploration Vehicle Test Article Installed in Tunnel 16T HAAS Cart.

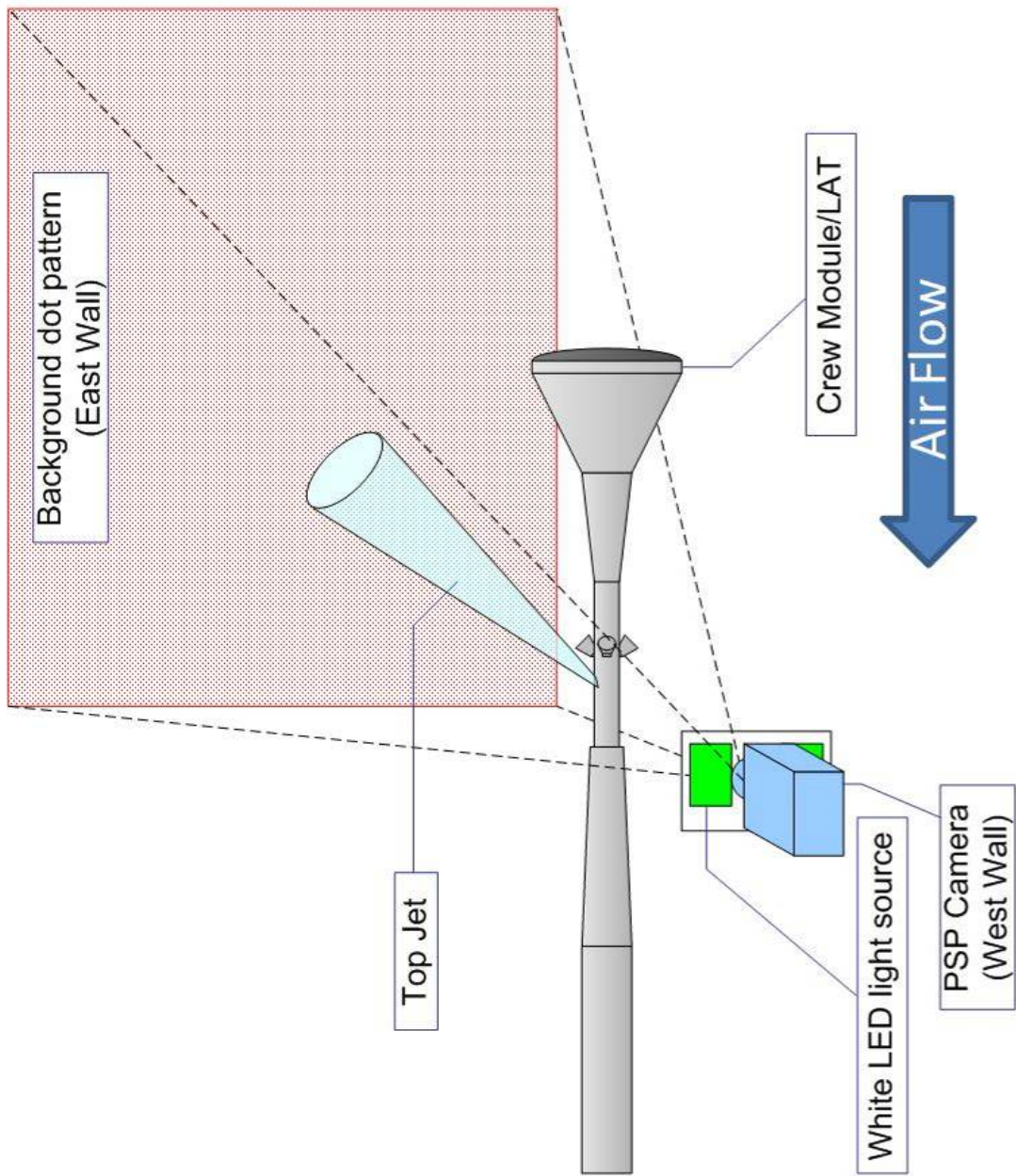


Figure 3. BOS System Configuration.

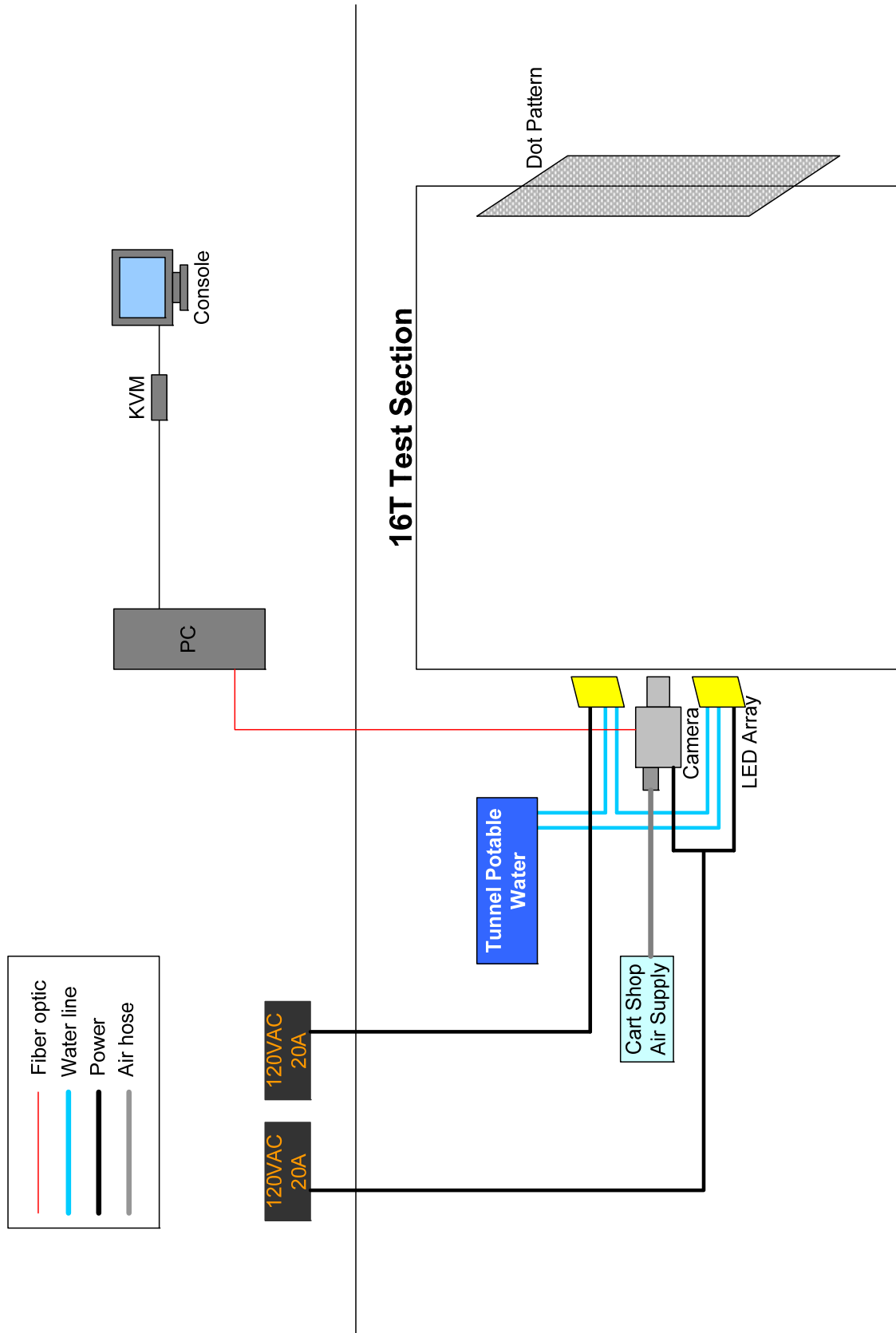
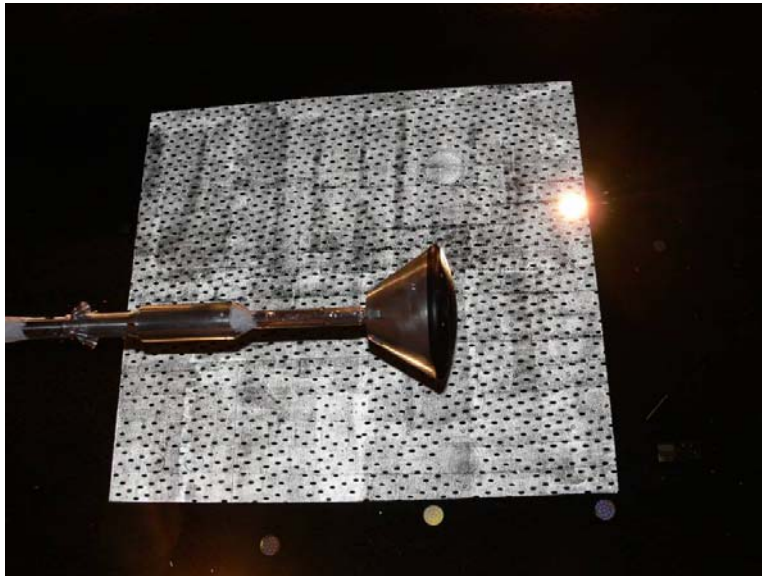


Figure 4. BOS System Schematic Looking Downstream.



a. Model Configuration 101 in Front of the Dot Pattern on the East Wall.



b. Camera and LED Arrays in the West Wall Optical Port.

Figure 5. BOS Installation Photos.

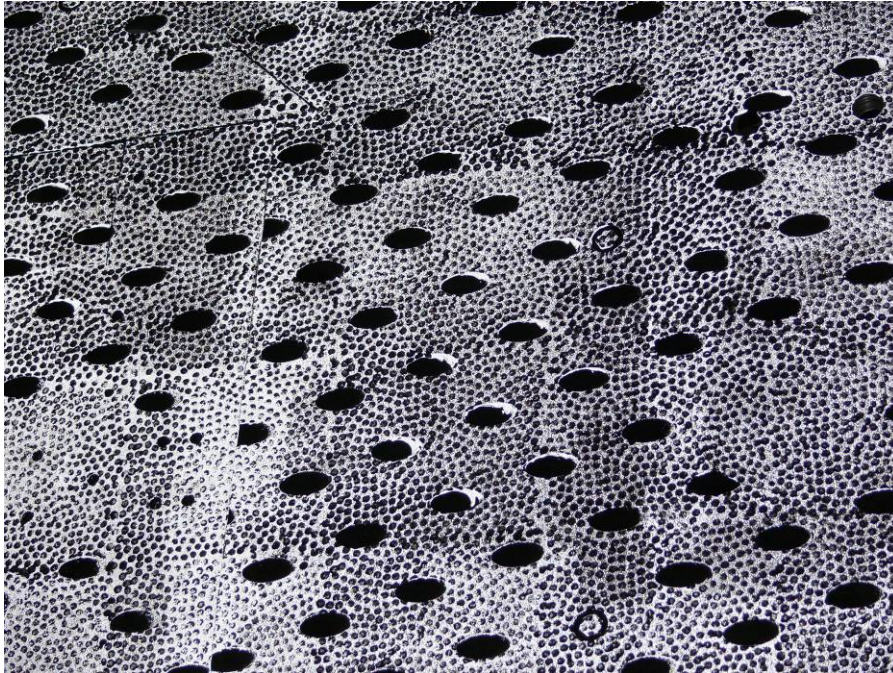
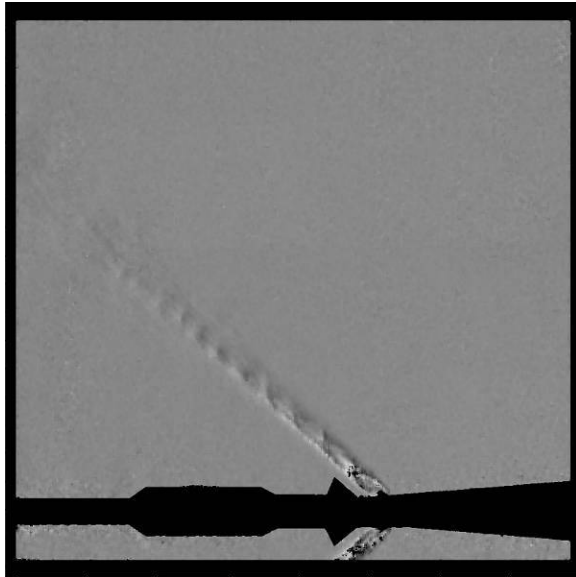
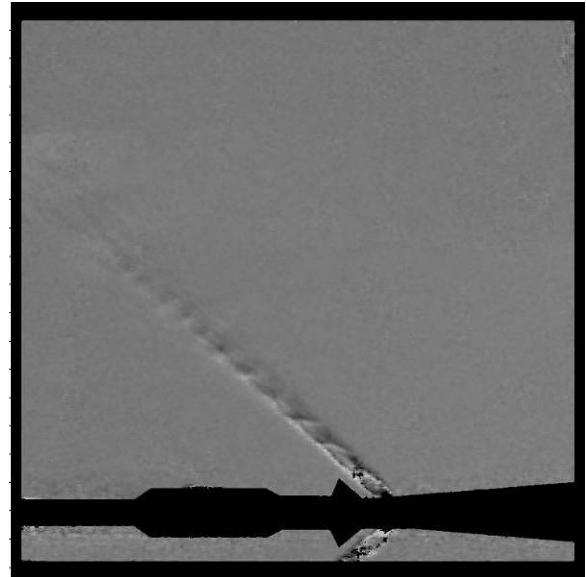


Figure 6. Close-Up Image of BOS Dot Pattern Applied to East Wall.

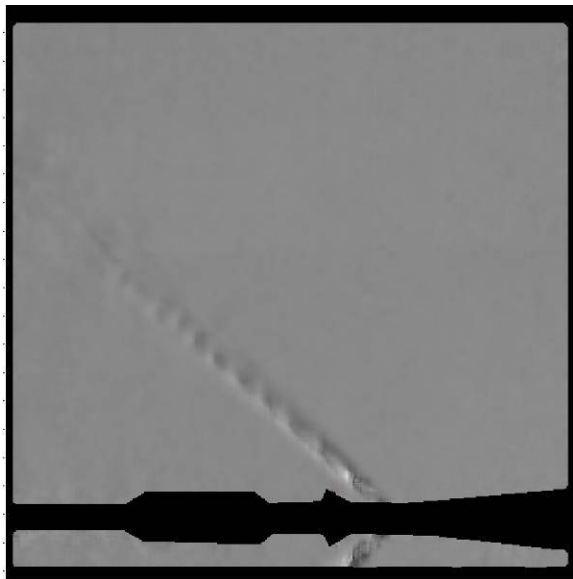


a. Vertical Knife-Edge (x-component)



b. Horizontal Knife-Edge (y-component)

Figure 7. Large JM (PTJM = avg) Nozzle BOS Visualization During Configuration 101 High-Pressure Air Checkout and Simulated Schlieren Images for a Multipass Processor Using a 32 x 32 Pixel Region at 50% Overlap Down to a 16 x 16 Pixel Region at 87% Overlap.

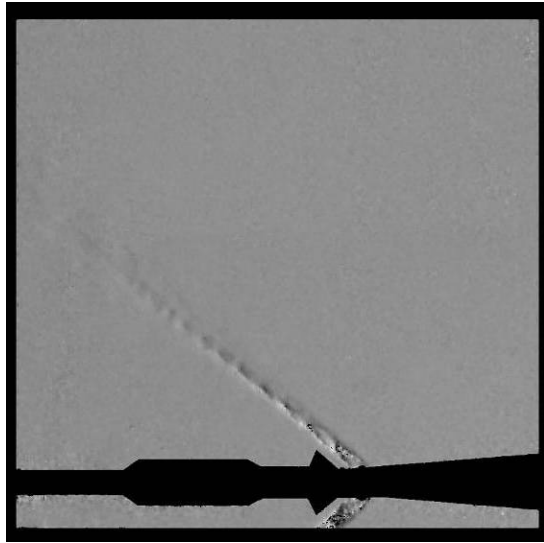


a. Vertical Knife-Edge (x-component)

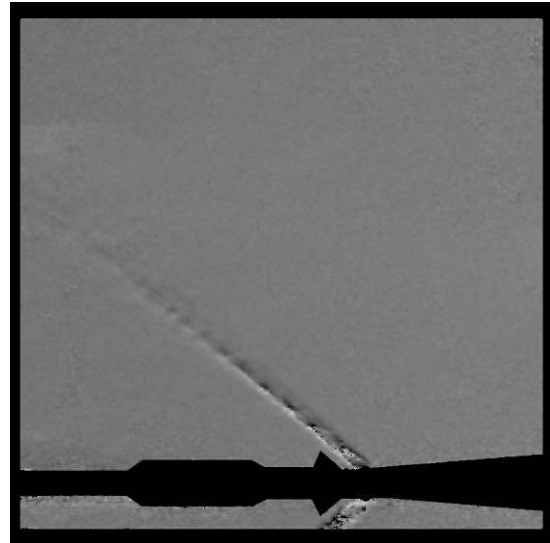


b. Horizontal Knife-Edge (y-component)

Figure 8. Large JM Nozzle (PTJM = avg) BOS Visualization During Configuration 101 High-Pressure Air Checkout and Simulated Schlieren Images for a Multipass Processor Using a 64 x 64 Pixel Region at 75% Overlap Down to a 32 x 32 Pixel Region at 87% Overlap.

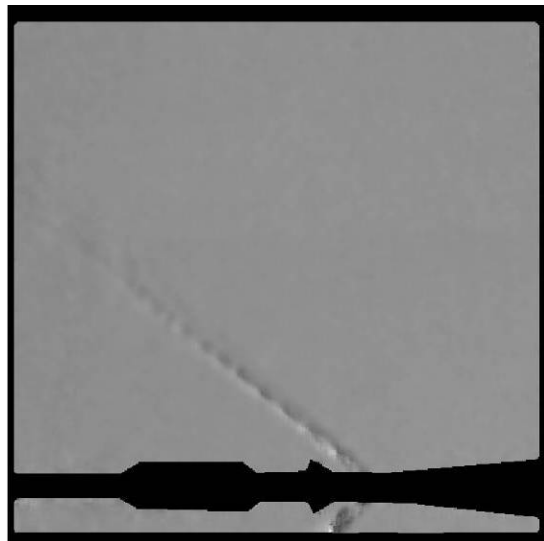


a. Vertical Knife-Edge (x-component)

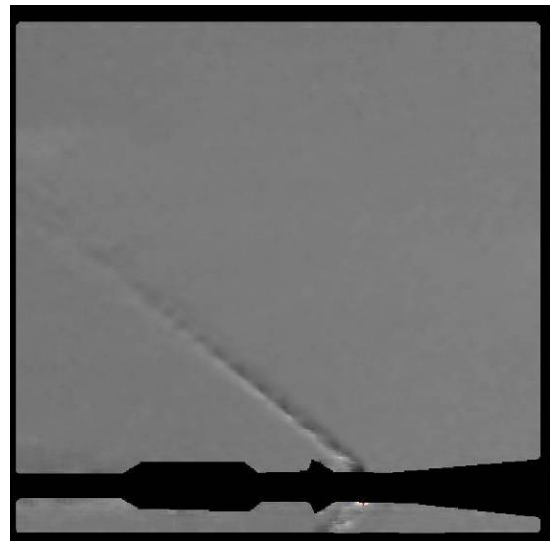


b. Horizontal Knife-Edge (y-component)

Figure 9. Small JM (PTJM = avg) Nozzle BOS Visualization During Configuration 101 High-Pressure Air Checkout and Simulated Schlieren Images for a Multipass Processor Using a 32 x 32 Pixel Region at 50% Overlap Down to a 16 x 16 Pixel Region at 87% Overlap.

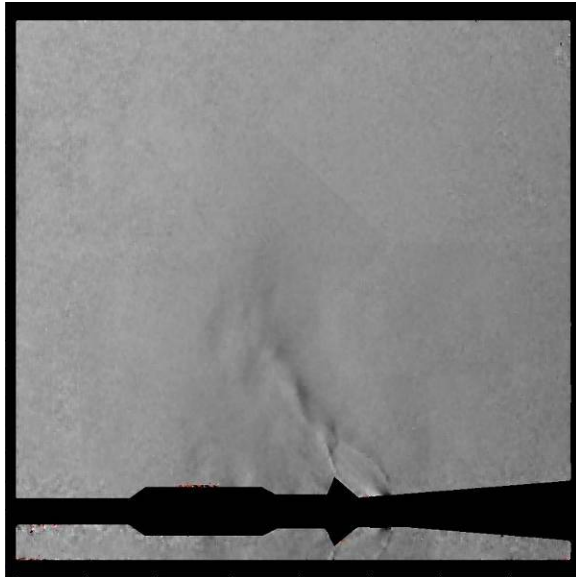


a. Vertical Knife-Edge (x-component)

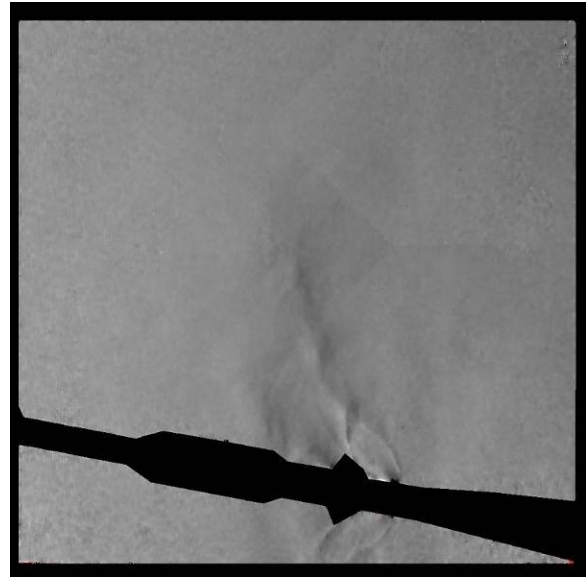


b. Horizontal Knife-Edge (y-component)

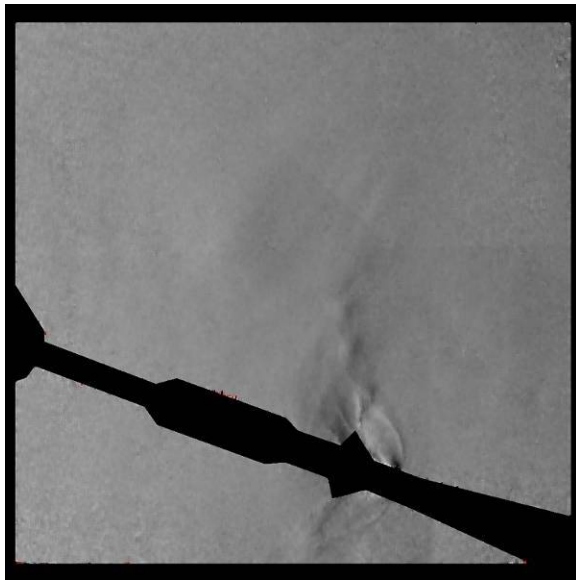
Figure 10. Small JM Nozzle (PTJM = avg) BOS Visualization During Configuration 101 High-Pressure Air Checkout and Simulated Schlieren Images for a Multipass Processor Using a 64 x 64 Pixel Region at 75% Overlap Down to a 32 x 32 Pixel Region at 87% Overlap.



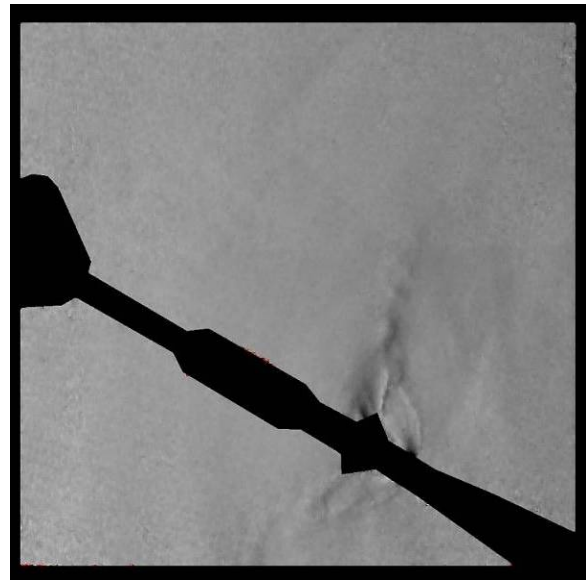
a. $\alpha = 180$ deg



b. $\alpha = 170$ deg



c. $\alpha = 160$ deg

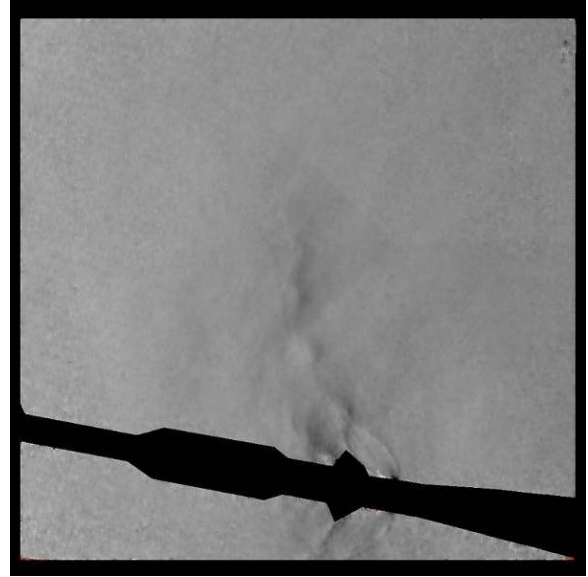


d. $\alpha = 150$ deg

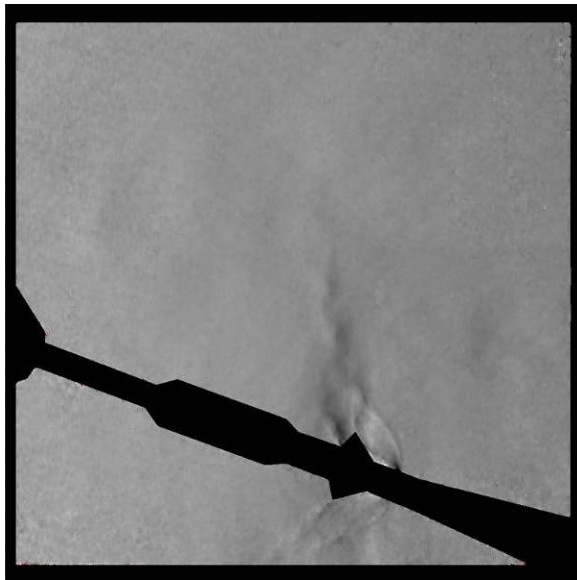
Figure 11. BOS Visualization of C101 Large JM Nozzle (PTJM = avg) at Mach 0.7 and 4 Model Attitudes. Processed with Mach 0.7 Jet-Off Background Image.



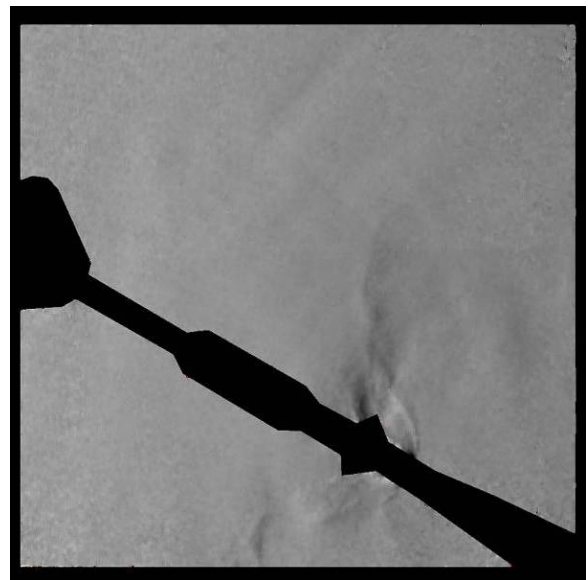
a. $\alpha = 180$ deg



b. $\alpha = 180$ deg

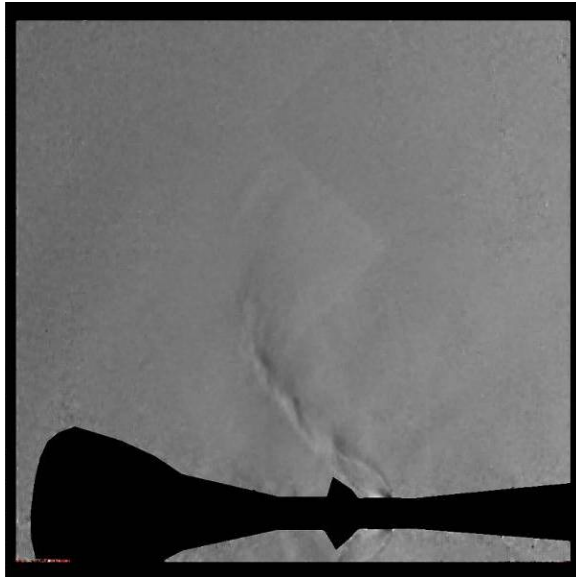


c. $\alpha = 180$ deg

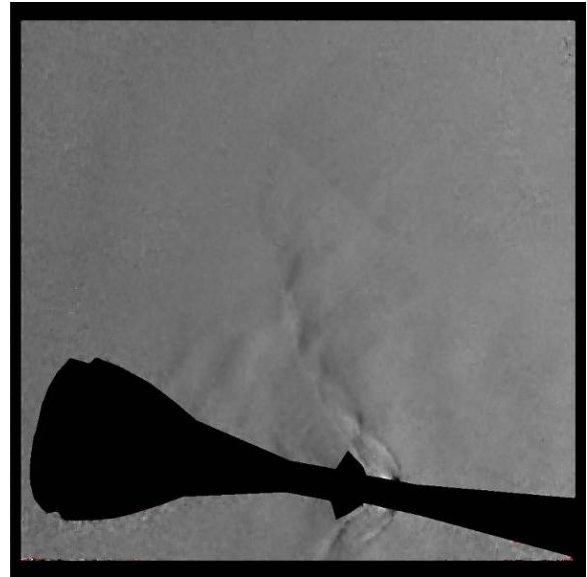


d. $\alpha = 180$ deg

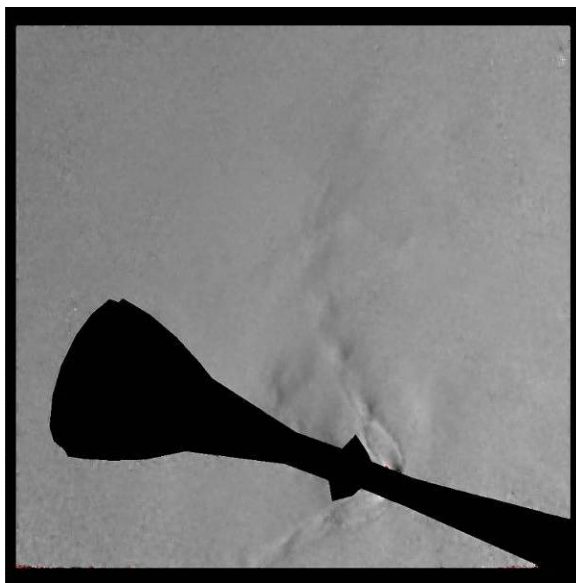
Figure 12. BOS Visualization of C101 Small JM Nozzle (PTJM = avg) at Mach 0.7 and 4 Model Attitudes. Processed with Mach 0.7 Jet-Off Background Image.



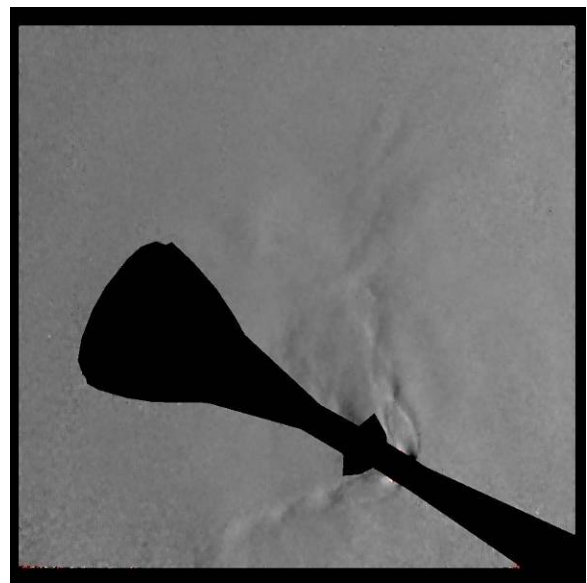
a. $\alpha = 180$ deg



b. $\alpha = 170$ deg

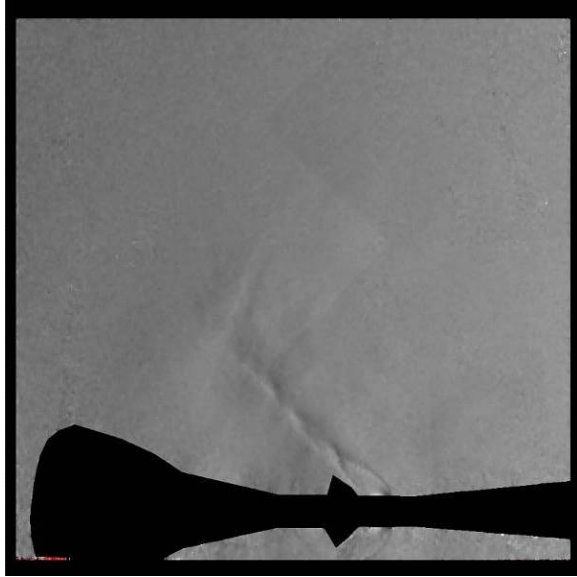


c. $\alpha = 160$ deg

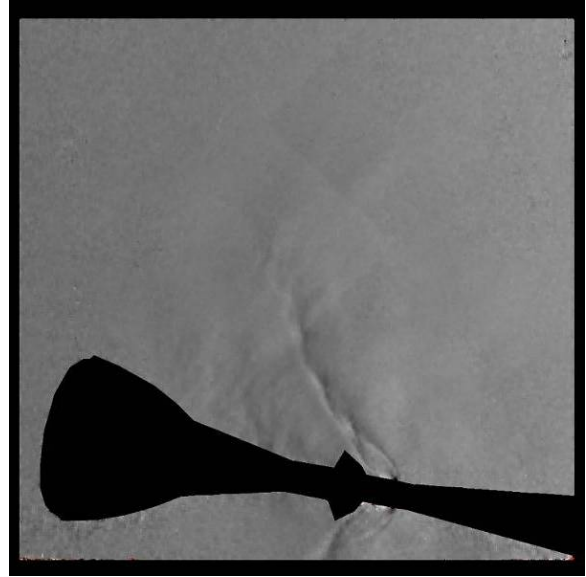


d. $\alpha = 150$ deg

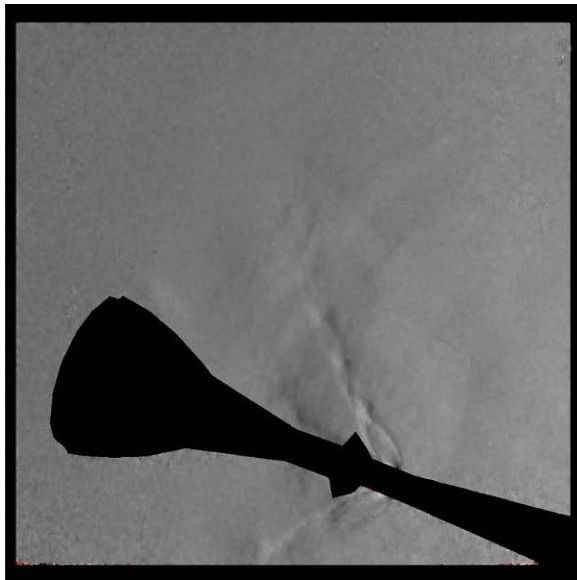
Figure 13. BOS Visualization of C103 Large JM Nozzle (PTJM = avg) at Mach 0.5 and 4 Model Attitudes. Processed with Mach 0.5 Jet-Off Background Image.



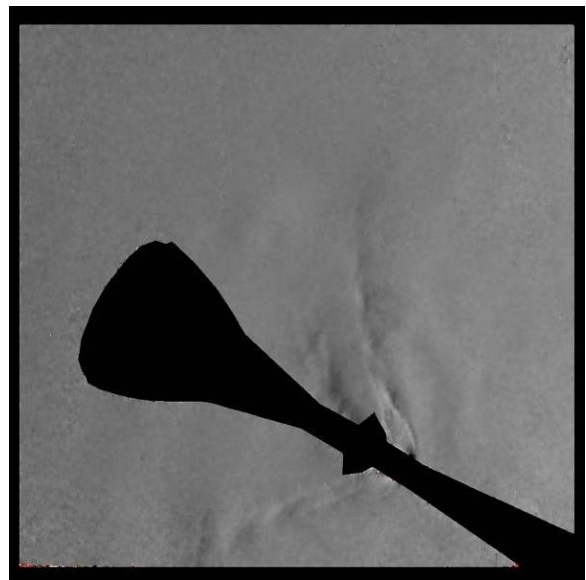
a. $\alpha = 180$ deg



b. $\alpha = 170$ deg

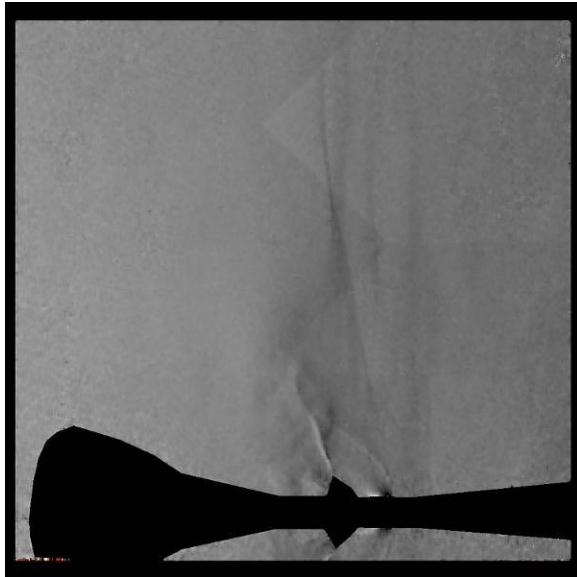


c. $\alpha = 160$ deg

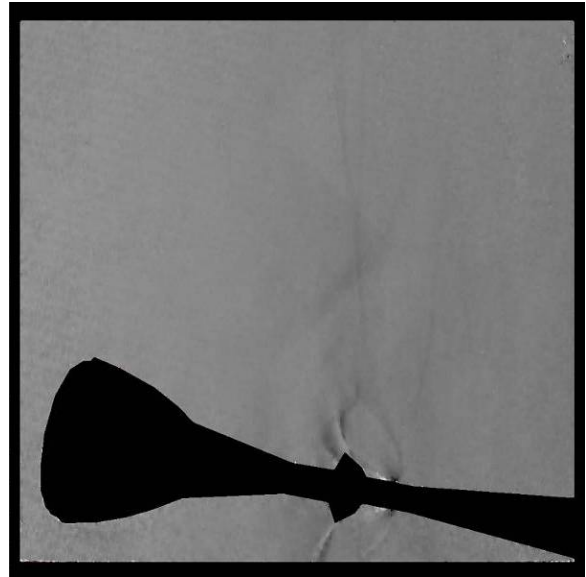


d. $\alpha = 150$ deg

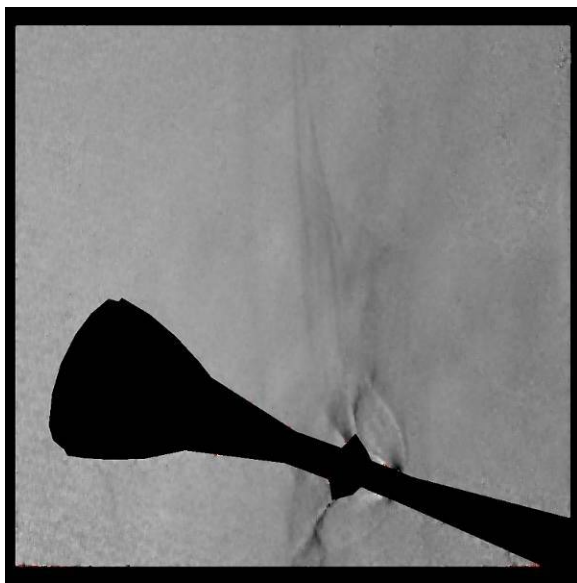
Figure 14. BOS Visualization of C103 Small JM Nozzle (PTJM = avg) at Mach 0.5 and 4 Model Attitudes. Processed with Mach 0.5 Jet-Off Background Image.



a. $\alpha = 180$ deg



b. $\alpha = 170$ deg

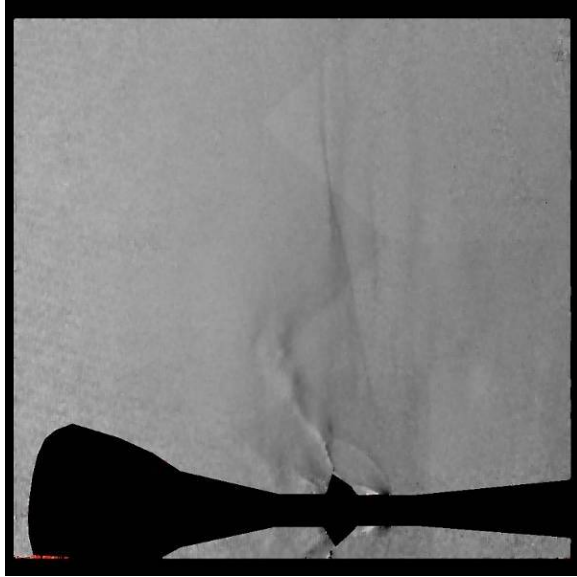


c. $\alpha = 160$ deg

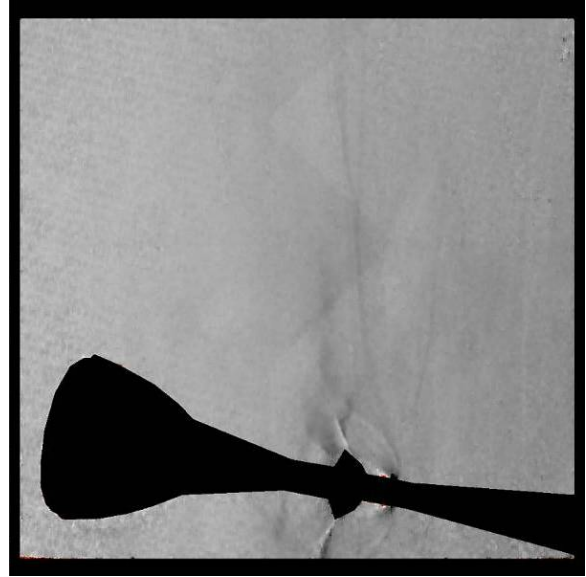


d. $\alpha = 150$ deg

Figure 15. BOS Visualization of C103 Large JM Nozzle (PTJM = avg) at Mach 0.9 and 4 Model Attitudes. Processed with Mach 0.9 Jet-Off Background Image.



a. $\alpha = 180$ deg



b. $\alpha = 170$ deg

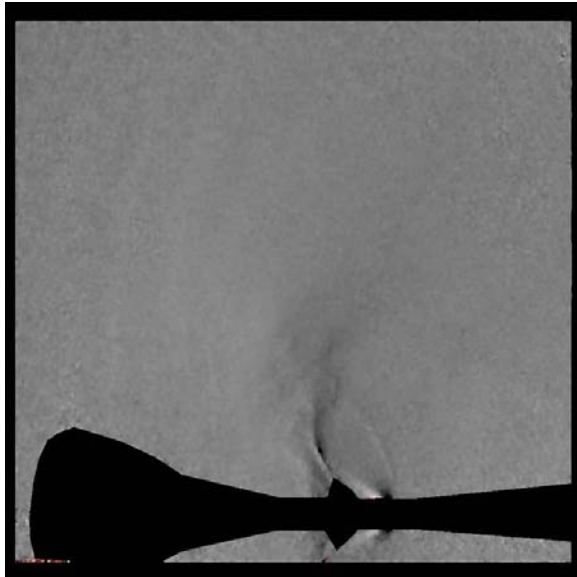


c. $\alpha = 160$ deg

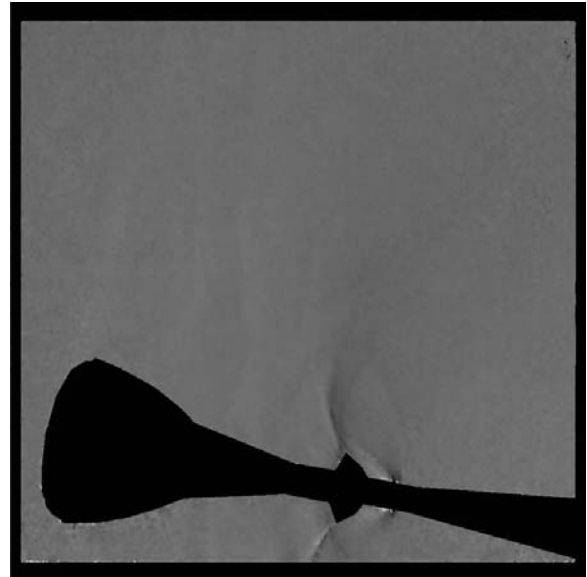


d. $\alpha = 150$ deg

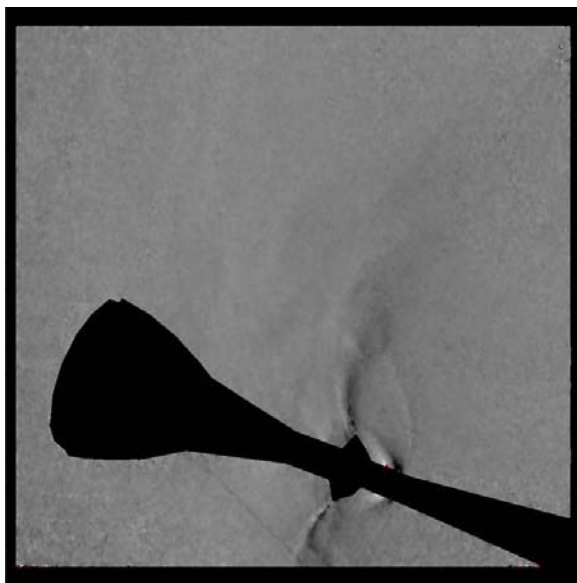
Figure 16. BOS Visualization of C103 Small JM Nozzle (PTJM = avg) at Mach 0.9 and 4 Model Attitudes. Processed with Mach 0.9 Jet-Off Background Image.



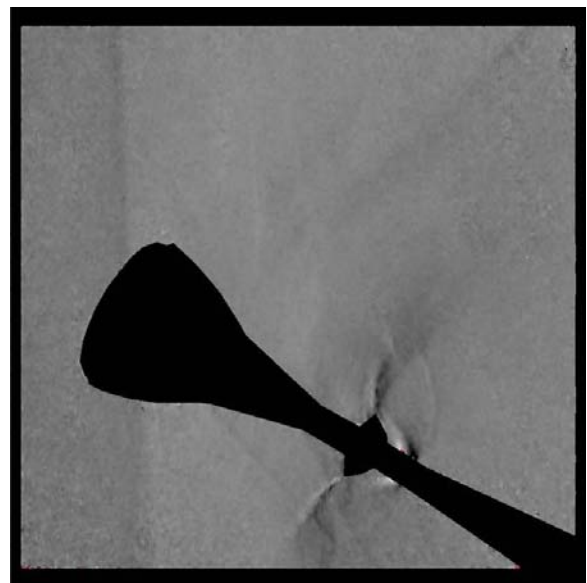
a. $\alpha = 180$ deg



b. $\alpha = 170$ deg

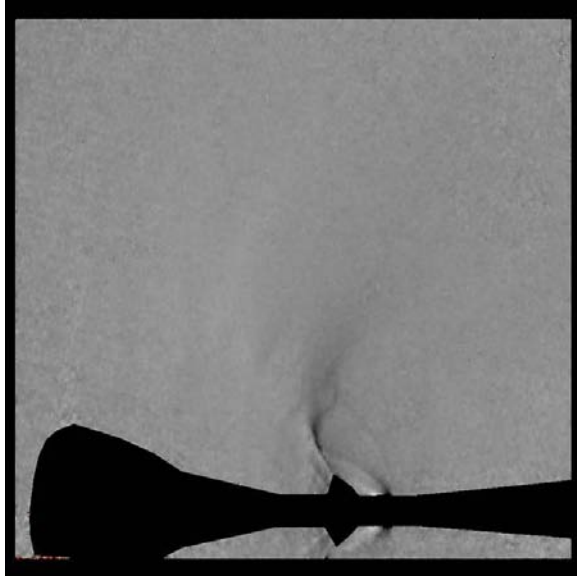


c. $\alpha = 160$ deg

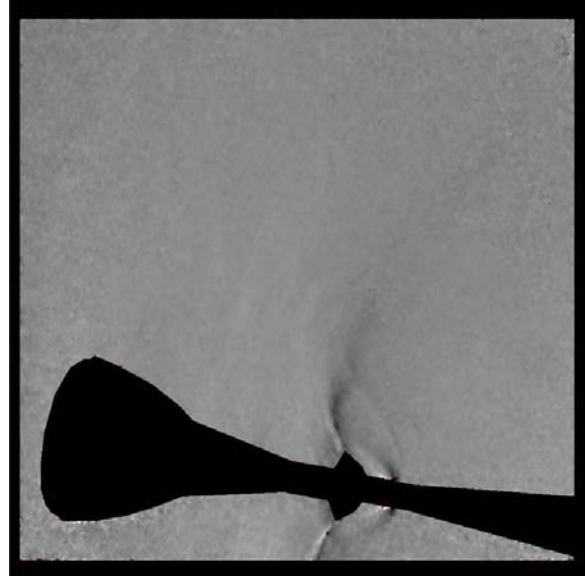


d. $\alpha = 150$ deg

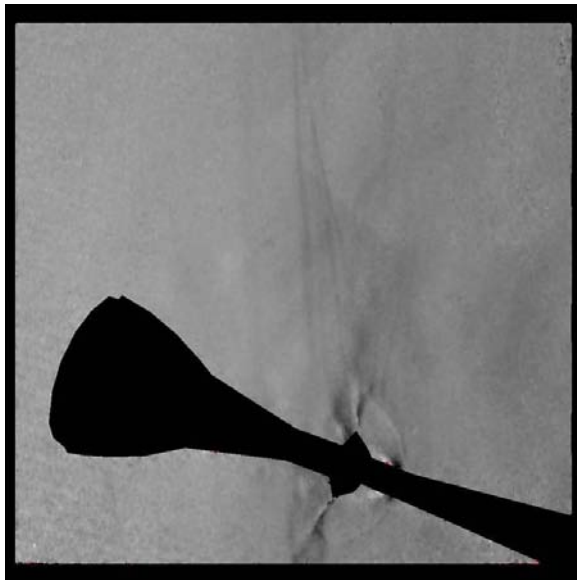
Figure 17. BOS Visualization of C103 Large JM Nozzle (PTJM = avg) at Mach 1.2 and 4 Model Attitudes. Processed with Mach 1.2 Jet-Off Background Image.



a. $\alpha = 180$ deg



b. $\alpha = 170$ deg

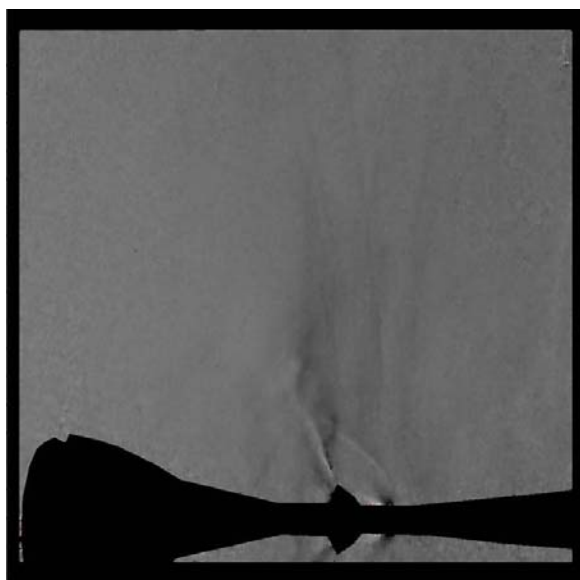


c. $\alpha = 160$ deg

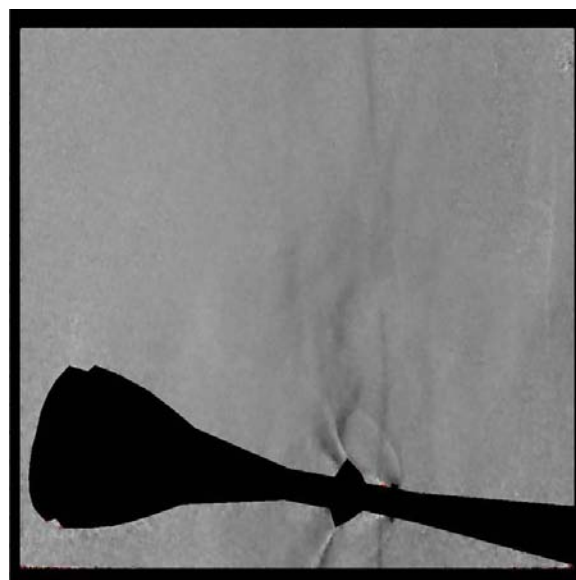


d. $\alpha = 150$ deg

Figure 18. BOS Visualization of C103 Small JM Nozzle (PTJM = avg) at Mach 1.2 and 4 Model Attitudes. Processed with Mach 1.2 Jet-Off Background Image.

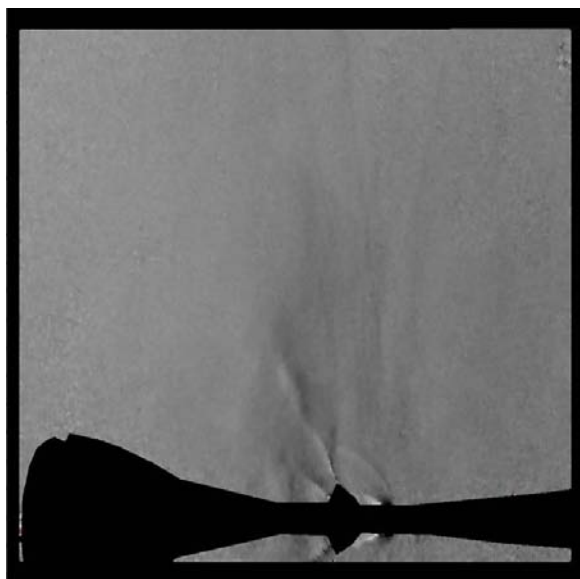


a. $\alpha = 180$ deg

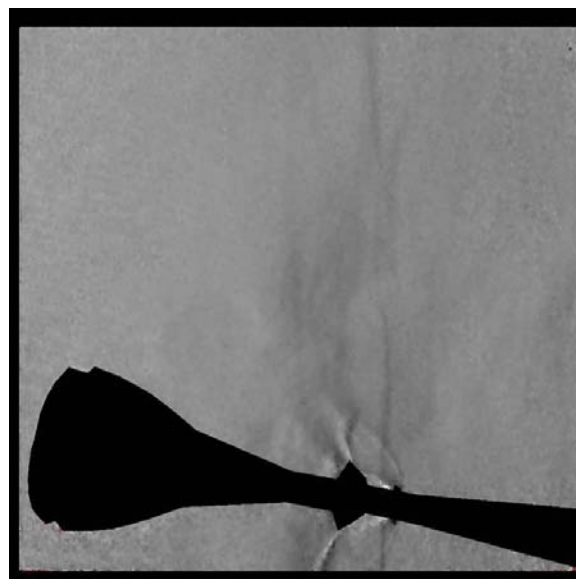


b. $\alpha = 170$ deg

Figure 19. BOS Visualization of C105 Large JM Nozzle (PTJM = avg) at Mach 0.9 and 2 Model Attitudes. Processed with Mach 0.9 Jet-Off Background Image.

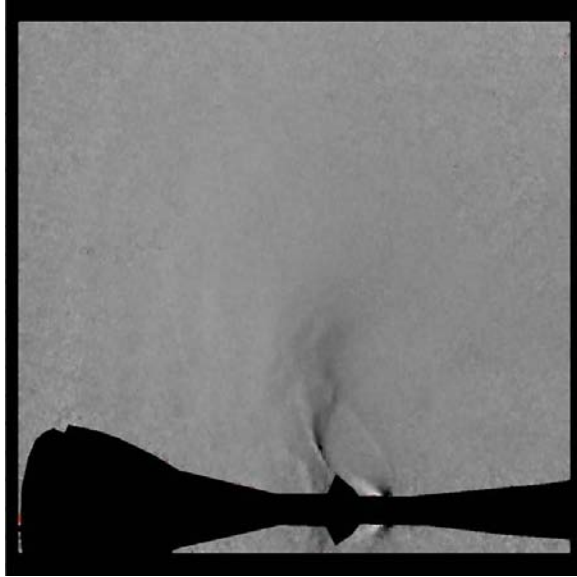


c. $\alpha = 160$ deg

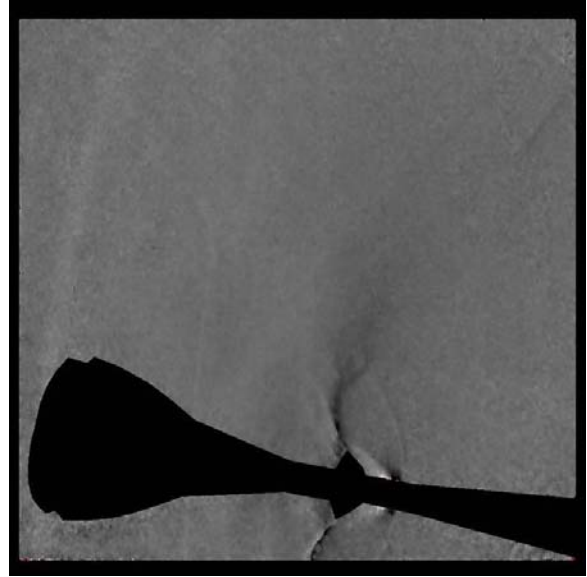


d. $\alpha = 150$ deg

Figure 20. BOS Visualization of C105 Small JM Nozzle (PTJM = avg) at Mach 0.9 and 2 Model Attitudes. Processed with Mach 0.9 Jet-Off Background Image.



a. $\alpha = 180^\circ$



b. $\alpha = 170^\circ$



c. $\alpha = 160^\circ$



d. $\alpha = 150^\circ$

Figure 21. BOS Visualization of C105 Large JM Nozzle (PTJM = avg) at Mach 1.2 and 4 Model Attitudes. Processed with Mach 1.2 Jet-Off Background Image.

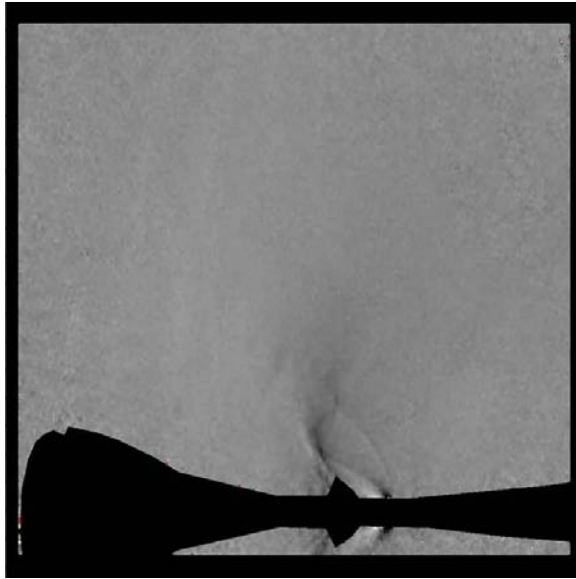
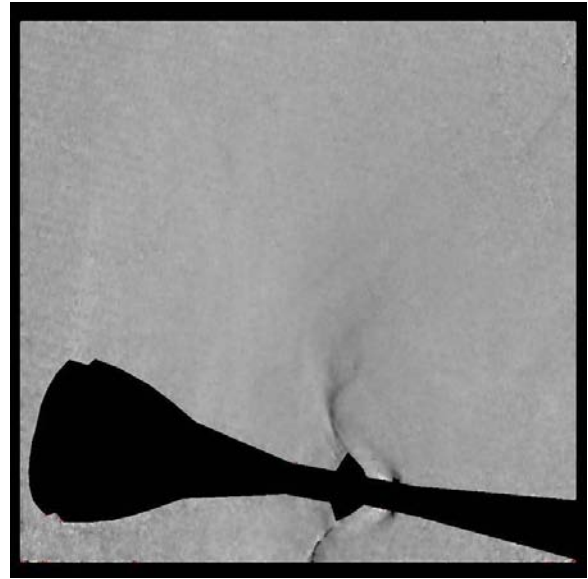
a. $\alpha = 180$ degb. $\alpha = 170$ deg

Figure 22. BOS Visualization of C105 Small JM Nozzle (PTJM = avg) at Mach 1.2 and 2 Model Attitudes. Processed with Mach 1.2 Jet-Off Background Image.

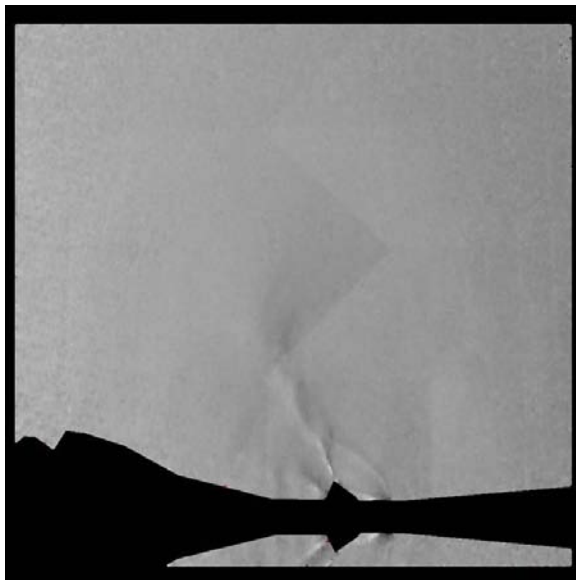
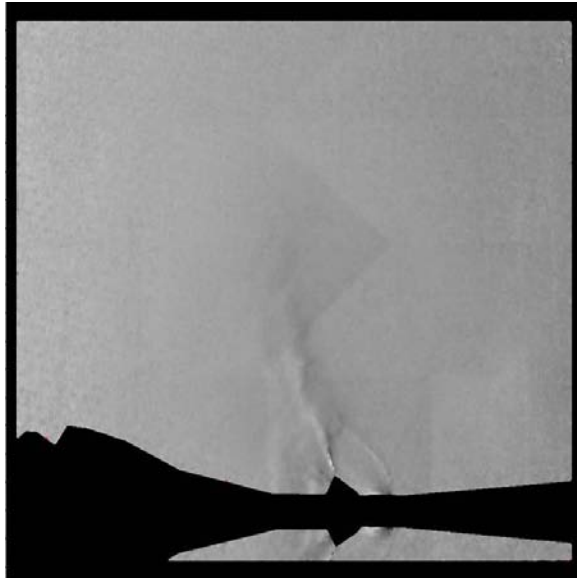
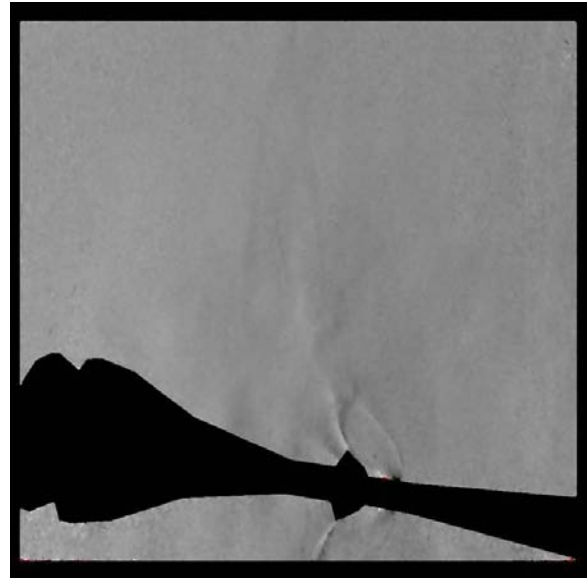
a. $\alpha = 180$ degb. $\alpha = 170$ deg

Figure 23. BOS Visualization of C106 Small JM Nozzle (PTJM = avg) at Mach 0.9 and 2 Model Attitudes. Image (a) was Processed Using the Atmosphere Jet-Off Background Image Due to Model Dynamics, While Image (b) Used the Mach 0.9 Jet-Off Background Image.



a. $\alpha = 180^\circ$



b. $\alpha = 170^\circ$

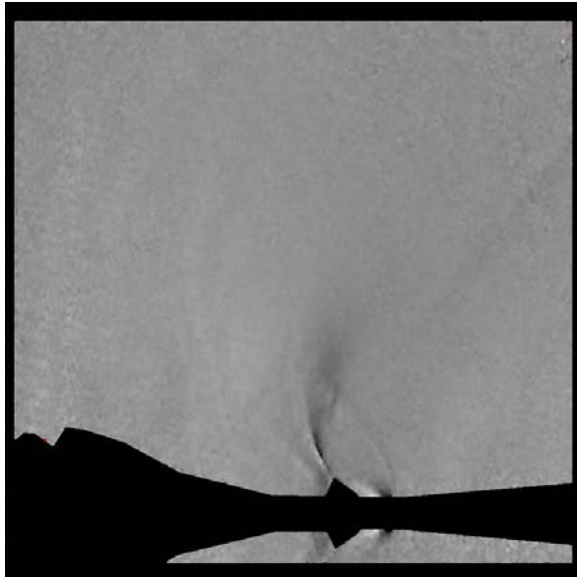


c. $\alpha = 160^\circ$



d. $\alpha = 150^\circ$

Figure 24. BOS Visualization of C106 Large JM Nozzle (PTJM = avg) at Mach 0.9 and 4 Model Attitudes. Image (a) was Processed Using the Atmosphere Jet-Off Background Image Due to Model Dynamics. Images (b)-(d) were Processed Using the Mach 0.9 Jet-Off Background Image.



a. $\alpha = 180$ deg



b. $\alpha = 170$ deg

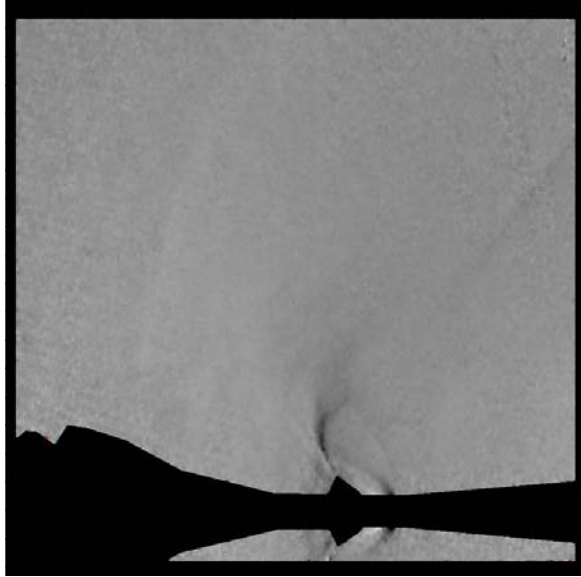


c. $\alpha = 160$ deg



d. $\alpha = 150$ deg

Figure 25. BOS Visualization of C106 Large JM Nozzle (PTJM = avg) at Mach 1.2 and 4 Model Attitudes. Processed with Mach 1.2 Jet-Off Background Image.



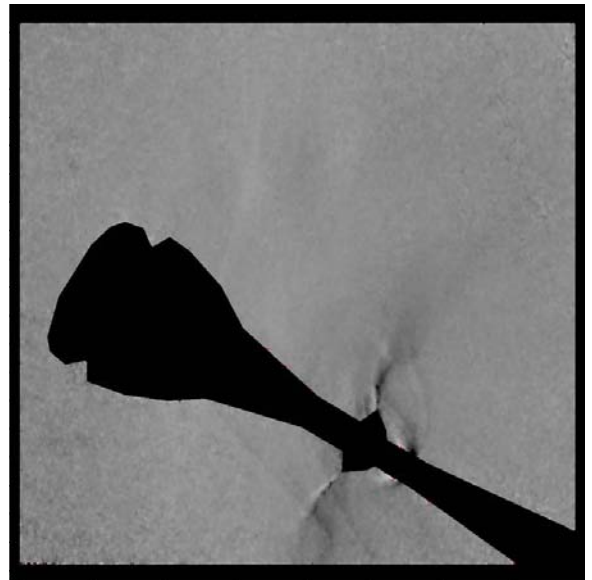
a. $\alpha = 180$ deg



b. $\alpha = 170$ deg

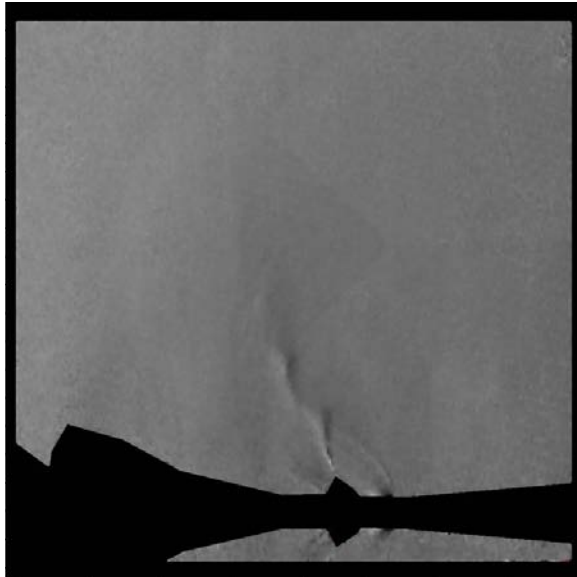


c. $\alpha = 160$ deg

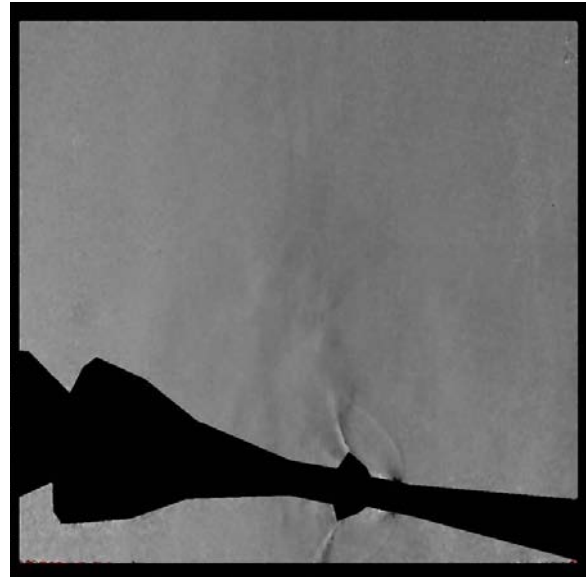


d. $\alpha = 150$ deg

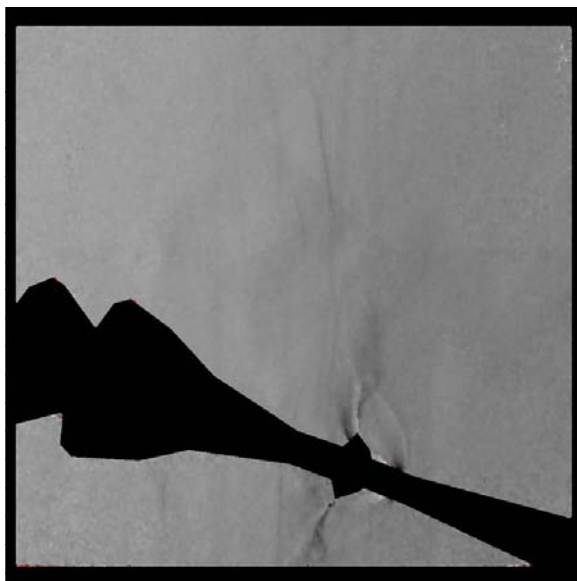
Figure 26. BOS Visualization of C106 Small JM Nozzle (PTJM = avg) at Mach 1.2 and 4 Model Attitudes. Processed with Mach 1.2 Jet-Off Background Image.



a. $\alpha = 180$ deg



b. $\alpha = 170$ deg



c. $\alpha = 160$ deg

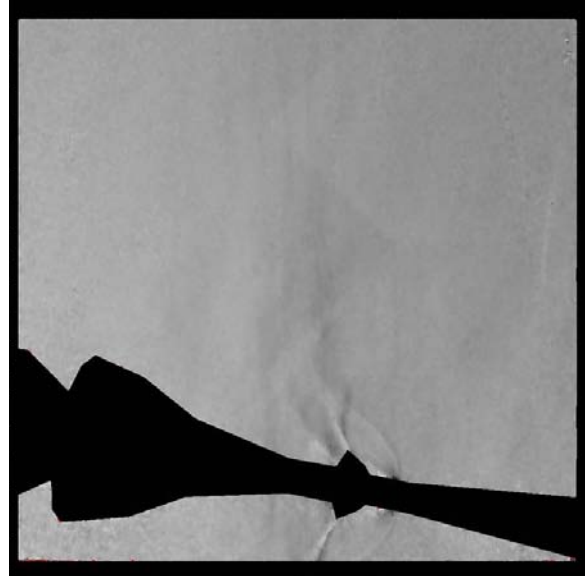


d. $\alpha = 150$ deg

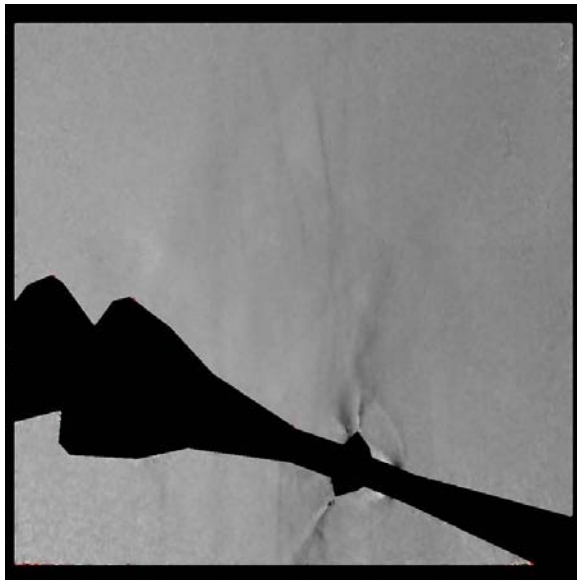
Figure 27. BOS Visualization of C107 Large JM Nozzle (PTJM = avg) at Mach 0.9 and 4 Model Attitudes. Processed with Mach 0.9 Jet-Off Background Image.



a. $\alpha = 180$ deg



b. $\alpha = 170$ deg

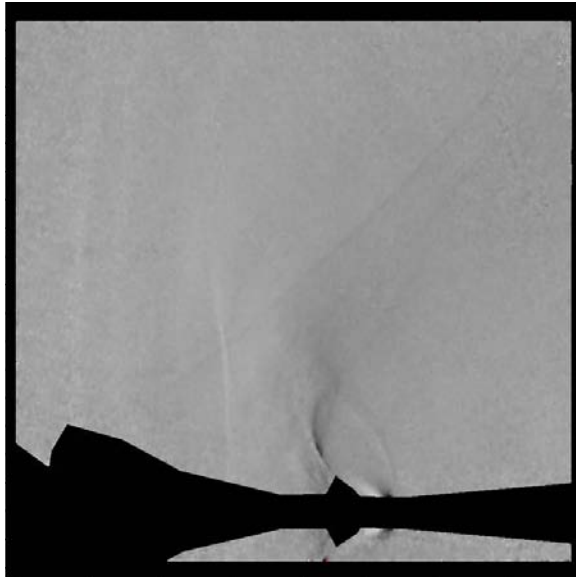


c. $\alpha = 160$ deg

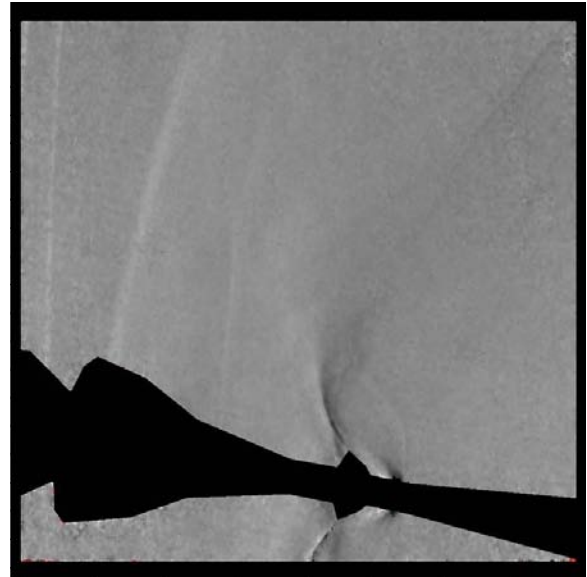


d. $\alpha = 150$ deg

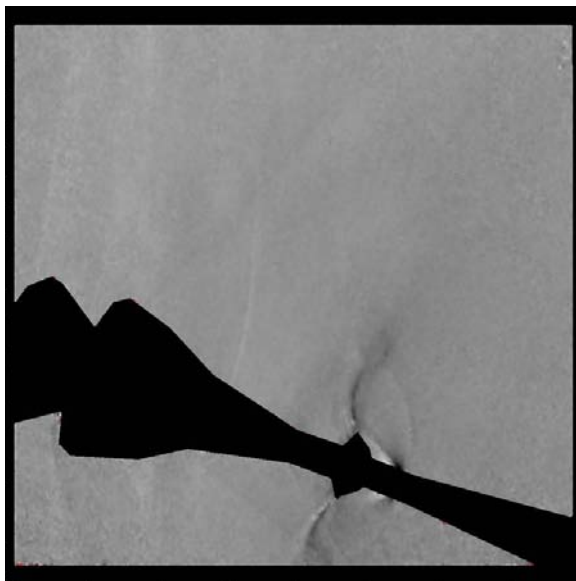
Figure 28. BOS Visualization of C107 Small JM Nozzle (PTJM = avg) at Mach 0.9 and 4 Model Attitudes. Processed with Mach 0.9 Jet-Off Background Image.



a. $\alpha = 180$ deg



b. $\alpha = 170$ deg

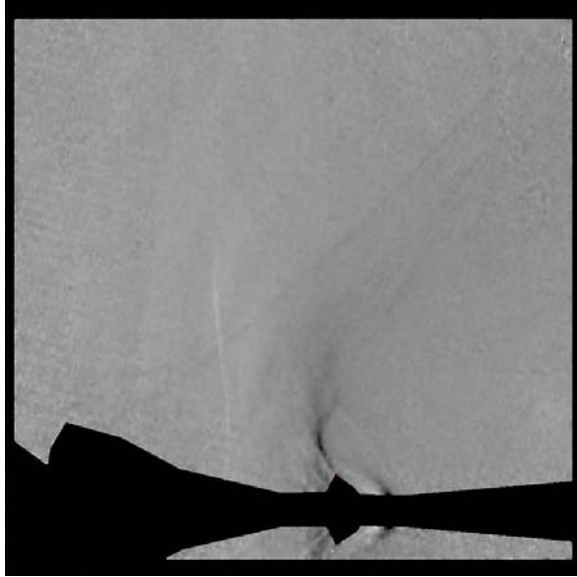


c. $\alpha = 160$ deg



d. $\alpha = 150$ deg

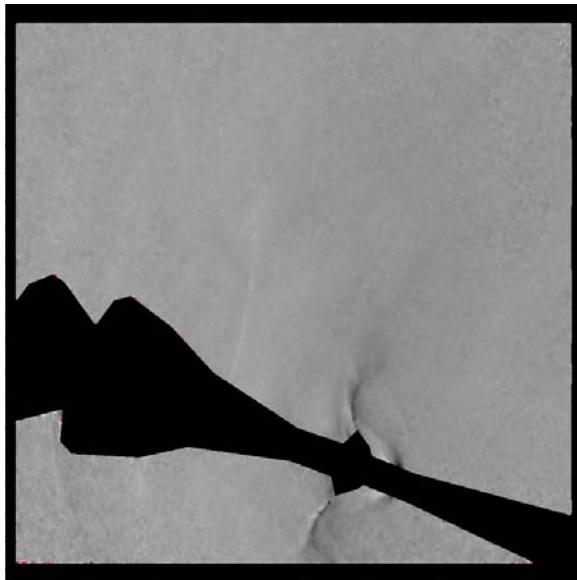
Figure 29. BOS Visualization of C107 Large JM Nozzle (PTJM = avg) at Mach 1.2 and 4 Model Attitudes. Processed with Mach 1.2 Jet-Off Background Image.



a. $\alpha = 180$ deg



b. $\alpha = 170$ deg

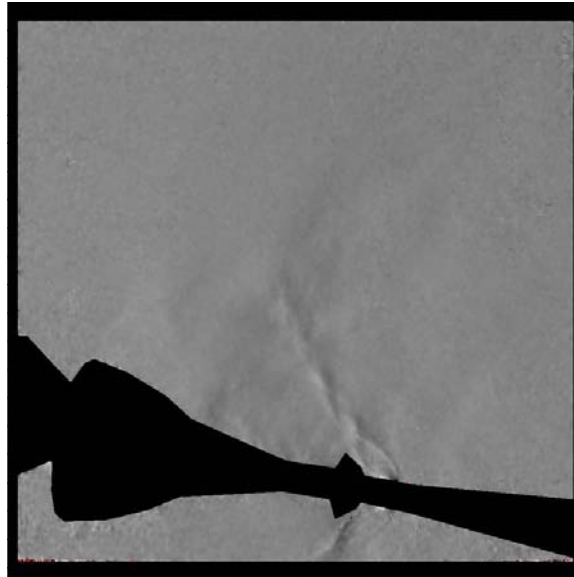


c. $\alpha = 160$ deg

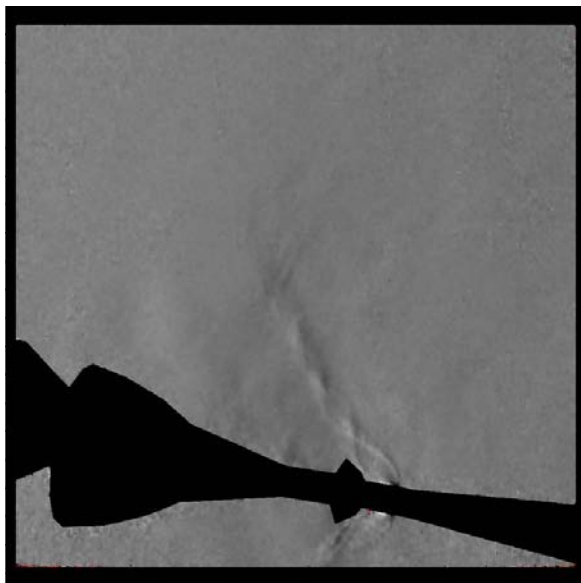


d. $\alpha = 150$ deg

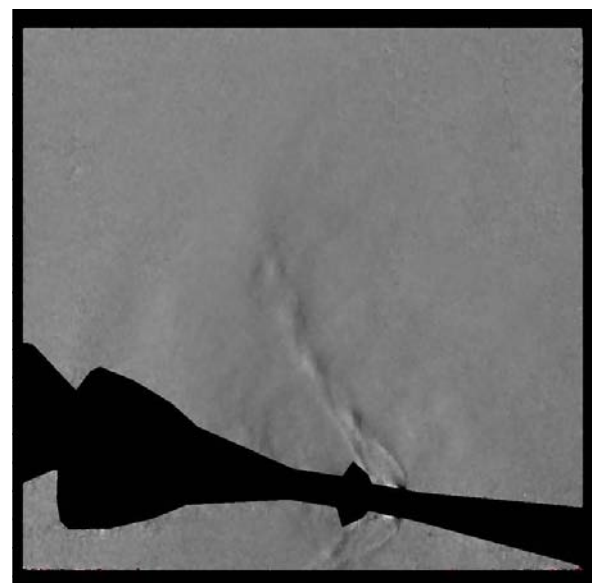
Figure 30. BOS Visualization of C107 Small JM Nozzle (PTJM = avg) at Mach 1.2 and 4 Model Attitudes. Processed with Mach 1.2 Jet-Off Background Image.



a. Minimum PTJM



b. Average PTJM



c. Maximum PTJM

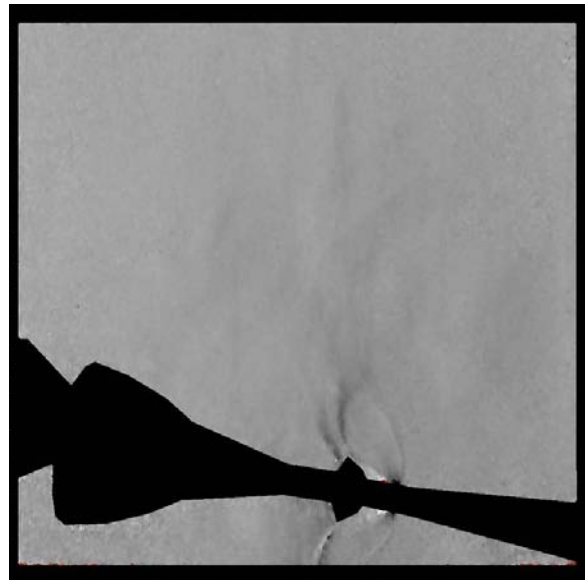
Figure 31. BOS Visualization of C109 Large JM Nozzle at Mach 0.5 and Pitched to 170 deg for 3 Nozzle Pressures. Processed with Mach 0.5 Jet-Off Background Image.



a. Minimum PTJM

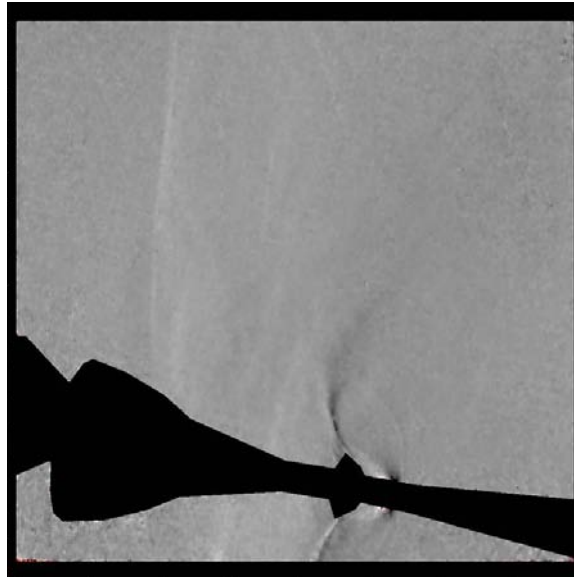


b. Average PTJM

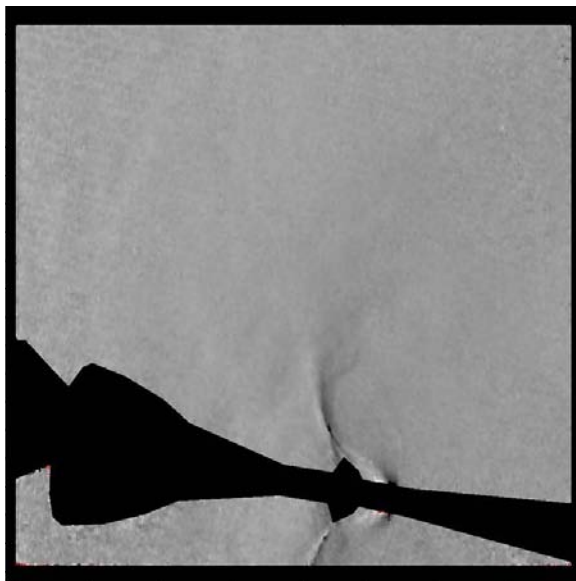


c. Maximum PTJM

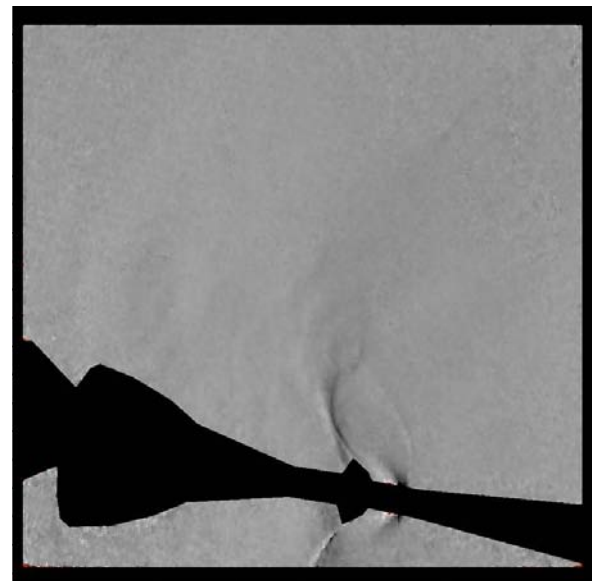
Figure 32. BOS Visualization of C109 Large JM Nozzle at Mach 0.9 and Pitched to 170 deg for 3 Nozzle Pressures. Processed with Mach 0.9 Jet-Off Background Image.



a. Minimum PTJM

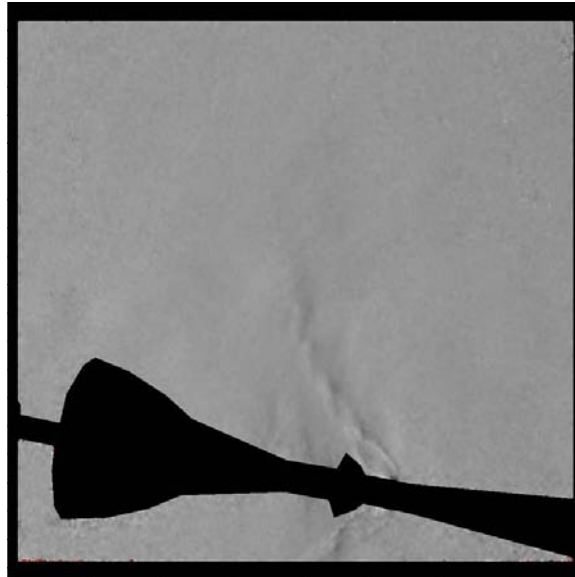


b. Average PTJM

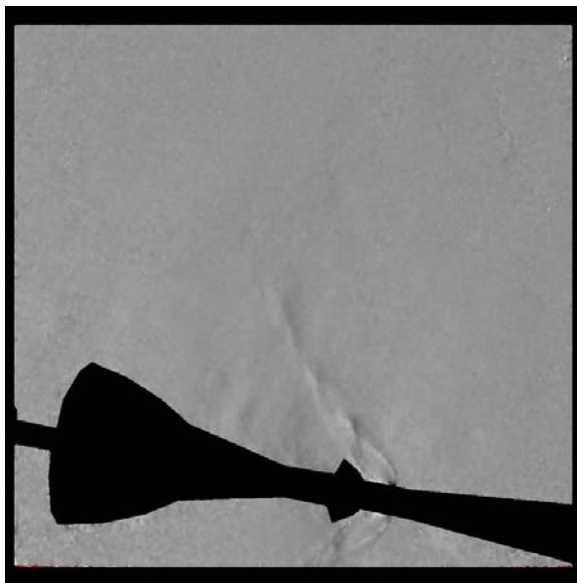


c. Maximum PTJM

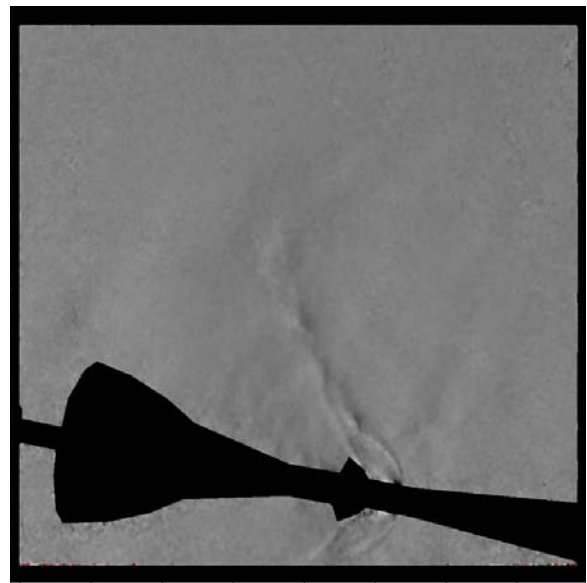
Figure 33. BOS Visualization of C109 Large JM Nozzle at Mach 1.2 and Pitched to 170 deg for 3 nozzle Pressures. Processed with Mach 1.2 Jet-Off Background Image.



a. Minimum PTJM

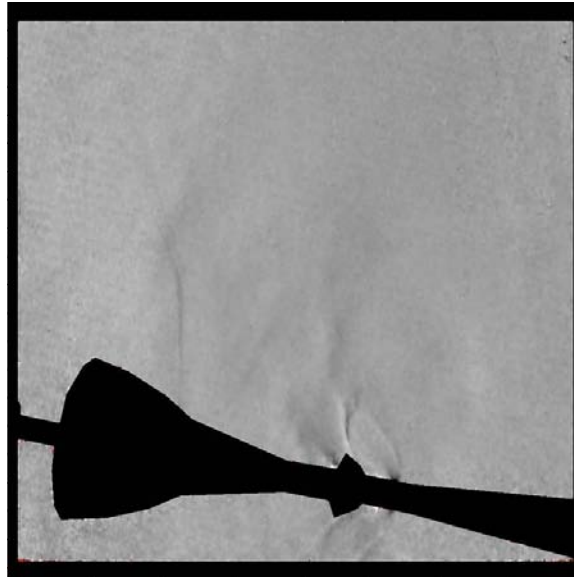


b. Average PTJM

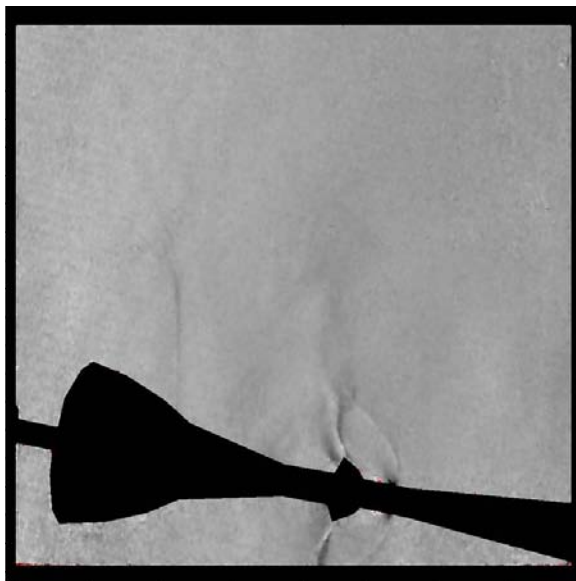


c. Maximum PTJM

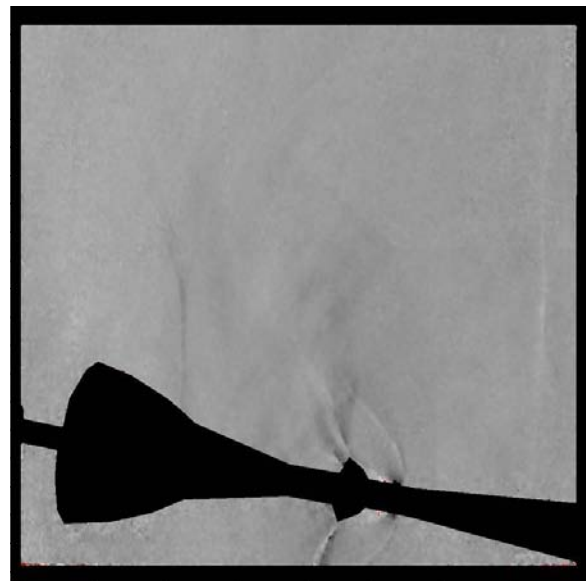
Figure 34. BOS Visualization of C111 Large JM Nozzle at Mach 0.5 and Pitched to 170 deg for 3 Nozzle Pressures. Processed with Mach 0.5 Jet-Off Background Image.



a. Minimum PTJM

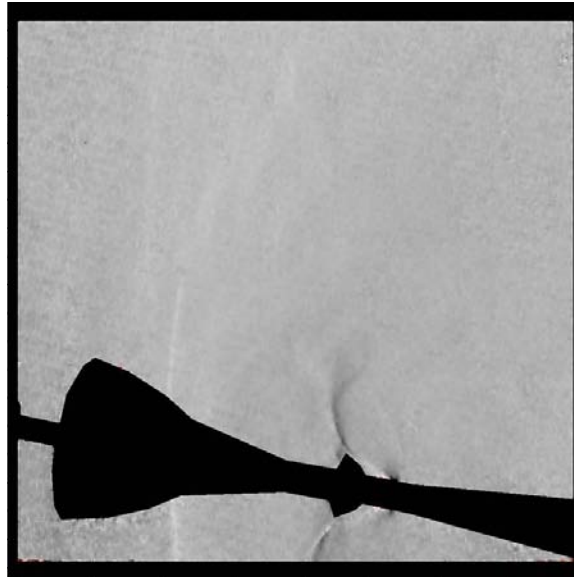


b. Average PTJM

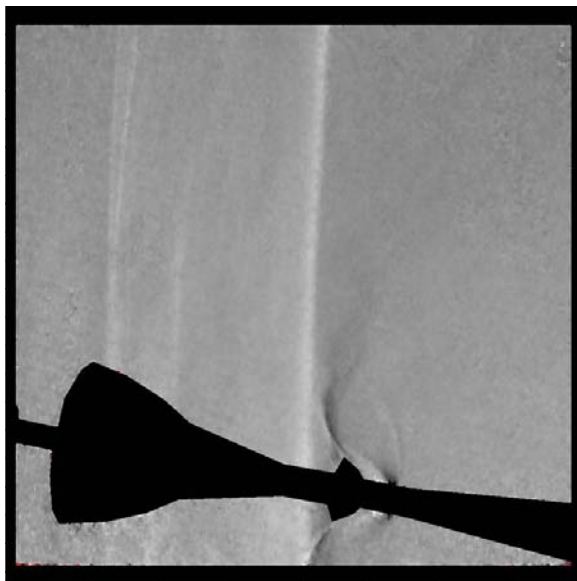


c. Maximum PTJM

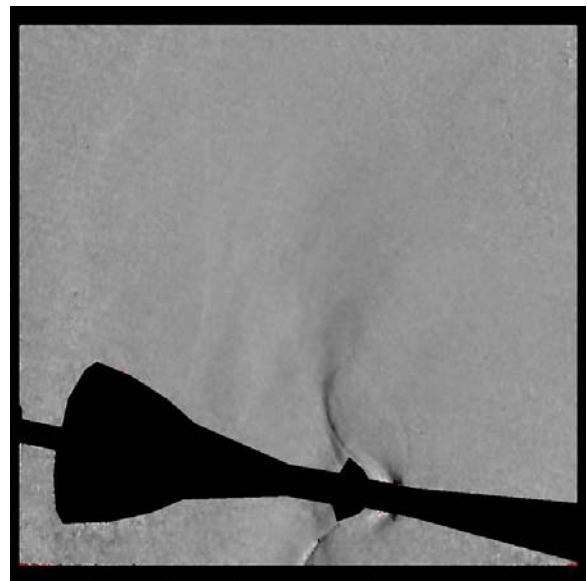
Figure 35. BOS Visualization of C111 Large JM Nozzle at Mach 0.9 and Pitched to 170 deg for 3 Nozzle Pressures. Processed with Mach 0.9 Jet-Off Background Image.



a. Minimum PTJM



b. Average PTJM



c. Maximum PTJM

Figure 36. BOS Visualization of C111 Large JM Nozzle at Mach 1.2 and Pitched to 170 deg for 3 Nozzle Pressures. Processed with Mach 1.2 Jet-Off Background Image.

Table 1. Nominal Test Conditions

Mach Number	Total Pressure, psfa	Total Temperature, °F	Static Pressure, psfa	Dynamic Pressure, psf	Reynolds Number, $\times 10^{-6}/ft$
0.00	2040	100	2040	0	0.0
0.50	700	100	590	103	1.0
0.70	578	100	417	143	1.0
0.90	510	100	301	171	1.0
1.20	479	100	198	199	1.0

Table 2. Run Number Summary

Config	PTJM	α	ϕ	Re/ft	Mach Number				
				$\times 10^{-6}$	0	0.5	0.7	0.9	1.2
101	off	180,170,160,150	0	1	968				
101	off	180,170,160,150	-135	1			1053		
101	avg	180,170,160,150	-135	1			1057		
101	avg	180,170,160,150	-225	1			1058		
101	avg	180	-225	1				1066	
101	avg	180	-225	1					1067
103	off	180,170,160,150	-135	1	1432/1433				
103	off	180,170,160,150	-135	1				1484	
103	avg	180,170,160,150	-135	1				1489	
103	avg	180,170,160,150	-225	1				1490	
103	off	180,170,160,150	-135	1					1550
103	avg	180,170,160,150	-135	1					1556
103	avg	180,170,160,150	-225	1					1557
103	off	180,170,160,150	-135	1		1596			
103	avg	180,170,160,150	-135	1		1606			
103	avg	180,170,160,150	-225	1		1607			
105	off	180,170,160,150	-135	1	1836				
105	off	180,170,160,150	-135	1				1843	
105	avg	180,170	-135	1				1845	
105	avg	180,170	-225	1				1846	
105	off	180,170,160,150	-135	1					1848
105	avg	180, 170	-135	1					1856
105	avg	180,170,160,150	-225	1					1857
106	off	180,170,160,150	-135	1	1992				

Config	PTJM	α	ϕ	Re/ft	Mach Number				
				$\times 10^6$	0	0.5	0.7	0.9	1.2
106	off	170,160,150	-135	1				2003	
106	avg	180,170,160,150	-135	1				2014	
106	avg	180,170	-225	1				2015	
106	off	180,170,160,150	-135	1					2049
106	avg	180,170,160,150	-135	1					2060
106	avg	180,170,160,150	-225	1					2061
107	off	180,170,160,150	-135	1	2197				
107	off	180,170,160,150	-135	1				2203	
107	avg	180,170,160,150	-135	1				2214	
107	avg	180,170,160,150	-225	1				2215	
107	off	180,170,160,150	-135	1					2252
107	avg	180,170,160,150	-135	1					2261
107	avg	180,170,160,150	-225	1					2262
109	off	170	-135	1	2607				
109	off	170	-135	1				1641	
109	min	170	-135	1				2646	
109	avg	170	-135	1				2651	
109	max	170	-135	1				2656	
109	off	170	-135	1					2686
109	min	170	-135	1					2692
109	avg	170	-135	1					2697
109	max	170	-135	1					2707
109	off	170	-135	1		2751			
109	min	170	-135	1		2757			
109	avg	170	-135	1		2763			
109	max	170	-135	1		2769			
111	off	170	-135	1	2929				
111	off	170	-135	1				3020	
111	min	170	-135	1				3021	
111	avg	170	-135	1				3029	
111	max	170	-135	1				3042	
111	off	170	-135	1					3088
111	min	170	-135	1					3074
111	avg	170	-135	1					3069
111	max	170	-135	1					3062
111	off	170	-135	1		3125			
111	min	170	-135	1		3096			
111	avg	170	-135	1		3101			
111	max	170	-135	1		3106			

APPENDIX A. LAMINA BL3000 SERIES LED SPECIFICATIONS

lamina®

Bright Lights. Bright Ideas.™

Brilliant Light!
BL-3000 SERIES

WHITE 4300K LED LIGHT ENGINE

Lamina Light Engines

As the market leader in the development and manufacture of super-bright LED arrays, Lamina brings solid state lighting to applications which until now were only possible with traditional lighting sources.

Lamina's LED arrays are manufactured by combining high brightness LEDs from industry-leading LED manufacturers with Lamina's proprietary packaging technology, multilayer Low Temperature Co-Fired Ceramic on Metal (LTCC-M). LTCC-M is a breakthrough in thermal performance for LED packaging technology, a key factor in determining LED life and reliability. Unmatched thermal performance coupled with package interconnectivity allows Lamina to densely cluster multiple LEDs to achieve exceptionally high luminous intensity in very small footprints. Lamina's arrays are available in white, RGB and monochrome, from 1W to 100W, and also are available in custom packages.

- HIGH LUMINOUS FLUX IN SMALL FOOTPRINT
- SUPERIOR THERMAL PERFORMANCE FOR IMPROVED RELIABILITY
- LONG LIFE AND HIGH LUMEN MAINTENANCE
- NO MERCURY OR LEAD
- CUSTOM SIZES AND SHAPES AVAILABLE

BL-3000 White

Lamina BL-3000 white LED arrays are configured with 39 cavities, each populated with multiple LEDs. Multiple LED die in each cavity, a unique feature made possible with Lamina's packaging technology, assure Lamina light engines deliver optimal color uniformity. Terminals are supplied with a solderable surface finish to enable users to connect arrays to driver circuitry or other arrays in a series or parallel circuit. The BL-3000 Series is the most powerful LED array on the market.

Lamina's white 4300K LED light engines are designed with an enhanced spectral distribution rich in red for applications demanding improved color rendition (90 typical CRI) and warmer color temperatures.



Typical Applications

GENERAL ILLUMINATION

- ARCHITECTURAL LIGHTING
- DECORATIVE AND ACCENT
 - COVE AND UNDER-SHELF
 - GARDEN AND PATHWAY

SIGNALS & SIGNAGE

- AIRFIELD TAXIWAY
- SECURITY
- BEACONS

TASK LIGHTING

MEDICAL

MACHINE VISION

To see how you can realize all these design benefits, to request a sample, or to speak with an engineer about your design, contact Lamina at 800.808.5822 or 609.265.1401 or visit www.laminaceramics.com.

[laminaceramics.com](http://www.laminaceramics.com)

lamina[®]

Bright Lights. Bright Ideas.™

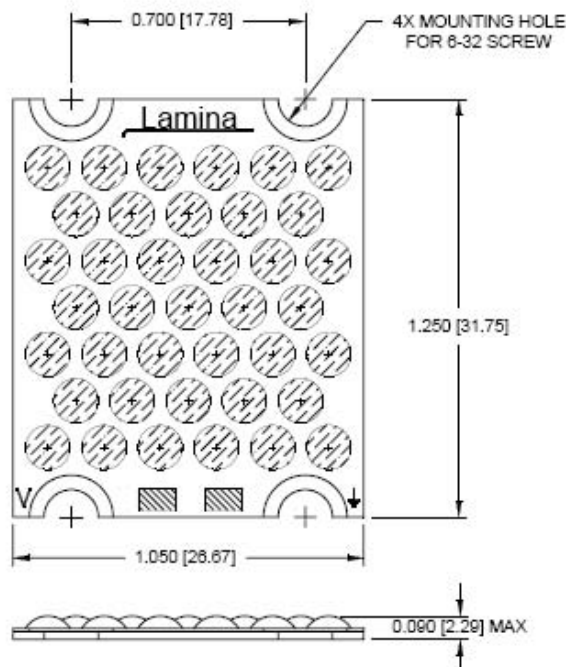
Technical Data

Part # BL-32D1-0245	Symbol	Min	Typical	Max	Unit
Color Temperature **	CCT	3500	4300	5500	°K
Voltage*	V_F	-	24	-	V
Test current	I_F	-	1.17	-	A
Power*	P	-	28	-	W
Luminous Flux*	Φ_V	510	525	-	lm
Thermal Resistance	T_R	-	0.66	-	°C/W

*Note 1. Optical and Electrical specifications are given for the specified drive current at a 25°C junction temperature.

**Note 2. Typical CRI is 90.

Mechanical Specifications



ATTACHMENT RECOMMENDATIONS

Lamina's BL-3000 Series is configured with solder pads compatible with Sn63 or Sn62 solder. As with many electrical devices, non-acid RMA type solder flux should be used to prepare the solder pads before application of solder. If wire attachment is performed with a soldering iron, care must be taken to minimize heat transfer to the die and minimize leaching of the solderable pads.

ASSEMBLY RECOMMENDATIONS

Lamina's BL Series Light Engines, are designed for attachment to heatsinks with conductive epoxy or screw down for flange mount devices with thermal grease in the joint.

For attachment using screws, a 6-32 UNC fillister head slotted machine screw, 18-8 SS is recommended. Maximum torque is 4 inch pounds (45 newton centimeter). Required flatness of surface light engine is mounted to is 0.001 inch/inch.

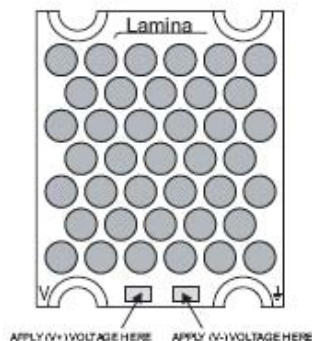
To see how you can realize all these design benefits, to request a sample, or to speak with an engineer about your design, contact Lamina at 800.808.5822 or 609.265.1401 or visit www.laminaceramics.com.

[laminaceramics.com](http://www.laminaceramics.com)

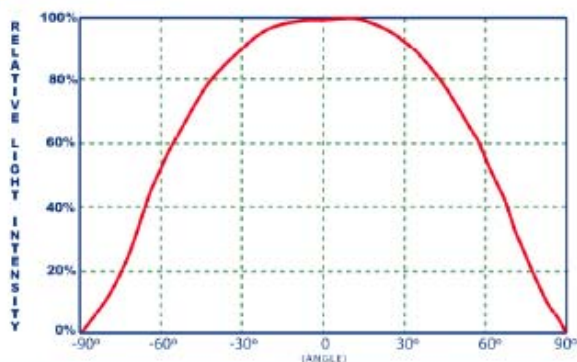
lamina®

Bright Lights. Bright Ideas.™

Electrical Connections



Typical Beam Pattern



HEAT SINK RECOMMENDATIONS

Lamina LED arrays provide efficient transfer of heat from the individual LED die to a customer supplied heat sink. All Lamina LED arrays must be operated at or below 125°C. A heat sink must be attached to the array with sufficient cooling capacity to keep the die junction below 25°C. The temperature rise from the array base to the die junction may be determined by calculating the product of the maximum package thermal resistance and the desired operating power level.

$$\text{Junction Temperature Rise (Tj (rise))} = \text{Operating Power (P)} \times \text{Lamina Array Thermal Resistance (Tr)}$$

The appropriate heat sink may then be determined by:

$$\text{Heat Sink Thermal Resistance (°C/W)} = (125 - \text{Tj (rise)} - \text{Maximum Ambient Temperature}) / \text{P}$$

OPTICAL RECOMMENDATIONS

Lamina LED arrays project a Lambertian radiation pattern, with projection angles built into the package cavity at approximately 125°. It will be necessary for users to create an optical reflector and lens structure that meets their light dispersion requirements. Please contact Lamina Application Engineering for support with your optical needs.

To see how you can realize all these design benefits, to request a sample, or to speak with an engineer about your design, contact Lamina at 800.808.5822 or 609.265.1401 or visit www.laminaceramics.com.

APPENDIX B. AXON RETROREFLECTIVE PAINT



AXON PRODUCTS

307 ECHELON ROAD • GREENVILLE, SC 29605
TEL. 864-299-2819 • FAX NUMBER 864-299-2820
E-MAIL: information@axon-aerospace.com

AEROSPACE TECHNICAL DATA

ALERT SERIES LIGHT REFLECTIVE COATING

January 1996
Revised: July 2004

PRODUCT DESCRIPTION:

This product is intended as a specialty coating for marking surfaces where night reflectivity is required. Alert provides reflective marking for steel, aluminum, concrete, and wood substrates. This product dries to a finish that reflects light back at the source.

SURFACE PREPARATION:

Surfaces to be painted should be clean and free of any soils or oil compounds. For best results, the surface should be lightly abraded before coating. For metal surfaces, areas which show corrosion or bare metal should be abraded to remove the corrosion before applying.

APPLICATION:

Mix Alert on a paint shaker before application. Proper mixing is very important to achieve optimum reflective properties. Alert can be applied by spraying, brushing, stenciling, or rolling. Best properties can be obtained by spraying with a tip size of .098 in. (2.5mm) with 25-50 psi. Apply in wet uniform coats until substrate is silver white in color. Extremely wet coats will not reflect as well as a drier coat. When rolling Alert, use a foam roller while rolling in one direction only. Do not apply Alert over latex coating or below 55°F. Odorless Mineral Spirits may be used as a reducer and for clean-up.

PHYSICAL PROPERTIES:

Appearance:	Available in various colors	
Weight per Gallon:	19.0#	
Fineness of Grind:	200 mesh	
Gloss:	5 max @ 60°	
Solids by Weight:	85.0%	
by Volume:	58.4%	
Volatile Organic Content:	2.85 lbs/gal or 342 g/L	
Coverage:	937 sq ft/gal @ 1 mil DFT	
Dry Time @ 1 mil DFT:	Tack Free:	1 - 2 hours
	Dry Hard:	24 hours
Shelf Life:	1 Year from Date of Manufacturing	
Storage Temperature:	40 - 95° F (4 - 35° C)	

PRECAUTIONS:

Use with adequate ventilation and proper safety equipment. See MSDS for complete details of composition and required precautions for safe use.



AXON PRODUCTS

307 ECHELON ROAD • GREENVILLE, SC 29605
 TEL. 864-299-2819 • FAX NUMBER 864-299-2820
 E-MAIL: information@axon aerospace.com

AEROSPACE TECHNICAL DATA

ALERT REFLECTIVE COATINGS MARCH-00

CODE/ALERT	DAYTIME COLOR	NIGHTTIME COLOR	CODE 3M "SCOTCHLITE"
1430	BLUE	BLUE	N/A
1440	SILVER	SILVER WHITE	7210
1441	SILVER	SILVER WHITE	N/A
1450	YELLOW	YELLOW	7211
1460	WHITE	SILVER WHITE	7216
1461	SILKSCREEN	WHITE	N/A
1462	RAILCAR WHITE	WHITE	N/A
1470	RED	RED	N/A
1480	BLACK	SILVER WHITE	7215
1490	GREEN	GREEN	N/A



JDL INDUSTRIES, INC.

Dade Phone: (305) 599-2022 / Fax: (305) 599-2078
 Broward Phone (954) 978-0046 / Fax: (954) 978-0710
 ATLANTA Phone (770) 840-0702 / FAX: (770) 840-0902

CUSTOMER REGISTRATION FORM

3M


CUSTOMER CODE: _____ DATE: ____/____/____

CORPORATE / COMPANY NAME: _____

PURCHASING AGENT: _____

PHONE: () _____ FAX: () _____

PURCHASING ADDRESS: _____

CITY, STATE, ZIP CODE: _____

E-MAIL: _____

A/P MANAGER: _____

PHONE: () _____ FAX: () _____

BILLING ADDRESS: _____

CITY, STATE, ZIP CODE: _____

WAREHOUSE MANAGER: _____

PHONE: () _____ FAX: () _____

SHIPPING ADDRESS: _____

CITY, STATE, ZIP CODE: _____

 CUSTOMER TYPE - PLEASE MARK ONE OF THE FOLLOWING:
 { AVIATION } { EXPORT } { GOVERNMENT } { MANUFACTURING }
 { MARINE } { REPAIR SHOP } { RESELLER } OTHER: _____

 CUSTOMER WISHES TO RECEIVE PROMOS ? Y / N (PLEASE CIRCLE CHOICE)

CUSTOMER SIGNATURE: _____

Please do not write below this line, for JDL use only:

J.D.L. REPRESENTATIVE: _____ REFERRAL CODE: _____



APPENDIX C. PHOTOMETRICS COOLSNAP K4 CAMERA



CoolSNAP_{K4} Monochrome

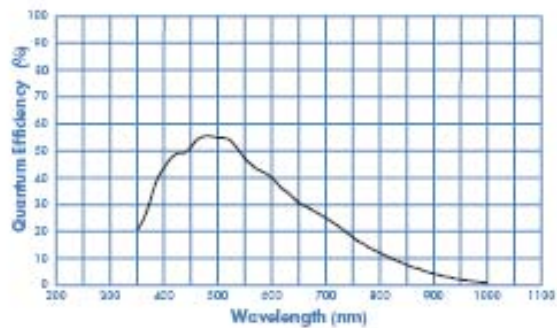
2048 x 2048 imaging array | 7.4 x 7.4- μ m pixels

The CoolSNAP_{K4} Monochrome camera from Photometrics® is a high-resolution digital imaging system designed for low-light scientific applications that require a large field of view. This cooled CCD camera system provides 12-bit digitization at 20 MHz. The large format of the CCD allows the user to image the microscope's whole field of view, while the small pixel size is ideally matched to the resolution limit of the microscope. The four-megapixel detector enables very fine image detail to be resolved, yet the pixels can be easily binned to improve sensitivity. New interline-transfer CCD technology provides high quantum efficiency.

Features	Benefits
20-MHz digitization	High-speed, high-sensitivity image capture
2048 x 2048 imaging array 7.4 x 7.4- μ m pixels	Resolves fine detail Ideally matched to optical microscope
Interline-transfer, progressive-scan CCD	Eliminates camera vibration and facilitates fast triggering
Flexible binning and readout	Increases light sensitivity while increasing the frame rate
12-bit digitization	Quantifies bright and dim signals in the same image
Thermoelectric cooling	Long integration times for higher sensitivity
Enhanced quantum efficiency	Provides higher sensitivity than typical interline cameras
C-mount	Easily attaches to microscopes, standard lenses, or optical equipment
Acquisition software	Captures, analyzes, and saves high-resolution images
PCI interface	High-bandwidth, uninterrupted data transfer
PVCAM® for Photometrics® Circular buffers Device sequencing	Supported by numerous third-party software packages Real-time focus Precise integration with shutters, filter wheels, etc. Compatible with Windows® 2000/XP, Mac OS X, and Linux® RH 9.0 (kernel version 2.4)

CoolSNAP_{K4} Mono Rev A1

Photometrics
CoolSNAP_{K4}



		Region		
		2048 × 2048	1024 × 1024	512 × 512
Binning	1 × 1	3	5	8
	2 × 2	5	8	10
	3 × 3	6	10	11
	4 × 4	8	11	12

(Frames per second)

Note: Frame rates are measured at 20 MHz with 0-second exposure times.

Specifications	
CCD image sensor	Kodak® KAI4020M; interline-transfer, progressive-scan device with microlenses
CCD format	2048 x 2048 imaging array 7.4 x 7.4-µm pixels 15.16 x 15.16-mm imaging area (optically centered)
Linear full well	30,000 e ⁻ (single pixel) 60,000 e ⁻ (2 x 2 binned pixel)
Read noise	≤10 e ⁻ rms @ 20 MHz
Nonlinearity	<1%
Digitizer type	12 bits @ 20 MHz
CCD temperature	-25°C (regulated)
Dark current	0.1 e ⁻ /p/s @ -25°C
Operating environment	0 to 30°C ambient, 0 to 80% relative humidity noncondensing
I/O	TTL (trigger/status): trigger, invert, inhibit, exposing, interline shift, frame readout 8-bit TTL (programmable) 8-bit DACs (two)

The diagram illustrates the system architecture. A microscope is connected to a camera, which is linked to an interface unit. This unit is connected to a computer system consisting of a tower and a monitor. The interface unit also has a fan and a power source.

Note: Specifications are typical and subject to change.



NOMENCLATURE

Alpha, α	Model angle of attack, deg
Phi, ϕ	Model roll angle, deg
BOS	Background-oriented schlieren
BPC	Boost protective cover
CCD	Charged coupled device
CEV	Crew Exploration Vehicle
CFD	Computational fluid dynamics
CM	Crew Module
Config	Model configuration number
F.S.	Model fuselage station, model scale in.
HAAS	High-angle automated sting
KVM	Keyboard, video, mouse
LAT	Launch abort tower
LED	Light emitting diode
Mach	Freestream Mach number
P	Pressure at wind-on condition, psfa
P_{∞}	Freestream static pressure, psfa
PCI	Peripheral Component Interconnect
PTJM	Jettison motor total pressure, psia
Re/ft	Freestream unit Reynolds number, ft^{-1}
Q_{∞}	Freestream dynamic pressure, psf
t	Time, sec
T.S.	Tunnel station, in.